

# We are IntechOpen, the world's leading publisher of Open Access books Built by scientists, for scientists

6,900

Open access books available

186,000

International authors and editors

200M

Downloads

Our authors are among the

154

Countries delivered to

TOP 1%

most cited scientists

12.2%

Contributors from top 500 universities



WEB OF SCIENCE™

Selection of our books indexed in the Book Citation Index  
in Web of Science™ Core Collection (BKCI)

Interested in publishing with us?  
Contact [book.department@intechopen.com](mailto:book.department@intechopen.com)

Numbers displayed above are based on latest data collected.  
For more information visit [www.intechopen.com](http://www.intechopen.com)



---

# Amorphous and Nanocrystalline Metallic Alloys

---

Galina Abrosimova and Alexandr Aronin

Additional information is available at the end of the chapter

<http://dx.doi.org/10.5772/64499>

---

## Abstract

In this chapter, evolution of structure and properties of amorphous alloys is discussed. Amorphous structure change before crystallization is analyzed for a lot of systems. Structure and property changes are discussed for both amorphous and amorphous-nanocrystalline materials. Nanocrystal formation in metallic glasses is considered at heating and deformation.

**Keywords:** metallic glasses, structure, properties, phase transformation, nanocrystalline structure

---

## 1. Introduction

Creation and development of modern technologies is based on fundamental research. Development of new materials is based on the knowledge of fundamentals of the processes that determine the formation of a material, as well as the correlation of structure and physical properties. Progress in the creation of new materials with certain properties (mechanical, electrical, magnetic) depends on the level of understanding of the processes that underlie the formation of a particular structure. The discovery and development of the materials with new physical properties, in turn, lead to the creation of new instruments and devices. Metallic glass and nanocrystalline metallic materials formed from metallic glasses, of course, apply to such materials.

Although many years passed after production of the first metallic glass, interest in them is only growing. In 1960, a group of researchers led by Professor Duwez first obtained metal alloy in a strange non-crystalline state [1]. X-ray diffraction patterns had no lines corresponding to whatever crystalline phases, and there was only a broad halo. This work [1] is considered to

be the first publication, which refers to amorphous metal alloys or metallic glasses. However, a year earlier Miroshnichenko and Sally [2] in Dnepropetrovsk (USSR) have already demonstrated the ability to produce metal alloys in a non-crystalline state. Obviously, due to not very popular scientific "Factory laboratory" journal, this work went unnoticed. Whatever it was, work [1] is considered to be the first publication devoted to the study of the amorphous phase in metallic systems (as opposed to, e.g., already investigated oxide systems). After the first publication, an avalanche of the works went; an amorphous phase could be obtained in a growing number of systems, and within few years the number of amorphous alloys was already counted in the hundreds. Interest in the metallic glass was due to their unusual structure, quite untypical of alloys, and a whole set of outstanding physical and chemical properties. Amorphous alloys may be high-strength, magnetically hard and soft magnetic, corrosion-resistant, and others. Thus, microhardness  $H_v$  of metallic glasses based on transition metals (Fe, Co, Ni) may exceed 1000, tensile strength may be greater than  $4.0 \text{ GN/m}^2$ . These values exceed the maximum values of strength and hardness of usual metals and alloys used in the industry. For example, the strength of the wire from iron-based metallic glasses is higher than the strength of piano wire [3]. Iron-based alloys have very good magnetic properties of low coercivity (0.5–1 A/m) and high saturation magnetization exceeding 1.4 T. Even higher hysteresis properties were obtained for  $\text{Co}_{70}\text{Fe}_5\text{Si}_{15}\text{B}_{10}$  [4] and Co-Fe-P-B [5] alloys that have almost zero magnetostriction. In general, the main characteristics of the soft magnetic amorphous alloys based on iron, cobalt, and nickel are the high values of residual induction and low magnetic reversal losses; high values of magnetic permeability (high iron content) or close to zero values of magnetostriction (high content of cobalt). Magnetic properties can also be increased with an addition of the alloying elements, the values of the magnetic permeability can be as high as 120,000 [6]. With a slight change in the composition, the properties of metallic glasses can vary quite significantly.

Most of the physical properties of solids are structurally sensitive. This dependence is typical for metallic glasses. For example, the soft magnetic properties of amorphous alloys can be improved by relaxation annealing, annealing in a magnetic field; mechanical properties naturally depend on the presence of residual stresses, corrosion properties depend on the chemical composition and state of the surface layer. Partially crystallized metallic glasses (peculiar composite consisting of amorphous and crystalline phases) have a number of very good properties that differ from the properties of both amorphous and crystalline materials. Importantly, the amorphous state is unstable; when heating or aging amorphous phase may decompose with a natural degradation of properties. Therefore, from the standpoint of basic science, and from the perspective of the industrial use of new materials, it is extremely important to study both the actual structure of the amorphous phase in metal alloys and its stability, the transition to the partially crystalline or fully crystalline state, as well as the correlation of structure and properties of the material.

The purpose of this review is to analyze the current state of research of structure evolution in amorphous and nanocrystalline metallic alloys. Particular attention is given to pre-crystallization processes and specific features of heterogeneous amorphous phase formation. The decomposition of homogeneous amorphous phase and the formation of regions with different

chemical compositions and/or different short-range order are considered for different types of metallic glasses. Formation of a nanocrystalline structure from homogeneous and heterogeneous amorphous phase is studied. Structure-property correlations are described.

## 2. Production of metallic glasses

The most common method of producing metallic glass or amorphous alloy is a melt quenching onto a moving substrate. When the melt is cooled, the cooling rate is about  $10^6$ – $10^9$  K/s (depending on the method of quenching). With such a large cooling rate at room temperature, the structure of liquid is frozen and the sample is non-crystalline.

Not all alloys can be obtained in an amorphous state. The most commonly considered three main criteria that determine diffusionless solidification [7]: thermodynamic criterion, morphological criterion and heat criterion. Usually kinetic and structural criteria are also discussed [8–10]. Some alloys may be prepared as amorphous will have less cooling rate [11–24].

## 3. Metallic glass structure

### 3.1. Main methods of structure investigation

The most common method for studying the structure of amorphous alloys is a method of large-angle X-ray scattering or as it is often simply called X-ray method [25, 26]. For detailed information about the structure of the amorphous phase, it is necessary to build the partial radial distribution functions [27–31]. At present, methods of construction of total and partial radial distribution functions are not used very often, although it should be noted the study of Mattern et al. [32] or the study cited in [33]. In analyzing the structure of metallic glasses, as a rule, with the help of Ehrenfest equation, the radius of the first coordination sphere as well as its changes at all types of influences are estimated; and distortion of diffuse maxima (the appearance of an additional shoulder, splitting of the peak, and others.) is determined. In combination with other methods of research, such an approach appears to be more productive.

Another commonly used method for analyzing the structure of the amorphous phase is the method of small-angle X-ray (SAXS) and neutron scattering [34]. The most important feature of this method is the possibility of studying heterogeneities in the structure of disordered systems as are metallic glass. In an absolutely homogeneous medium, there is no small-angle scattering, and the scattering pattern varies considerably with the appearance of any heterogeneities of the electron density in the structure.

In addition to the X-ray methods for studying the structure, the most important method is the transmission electron microscopy (TEM). Without dwelling on the specifics of the method, it is important to note that the analysis of the structure of amorphous phase is based on both electron diffraction and analysis of bright-field and dark-field TEM images. The high-resolution electron microscopy and micro- or nanobeam diffraction methods are used to study the

structural features of the early stages of crystallization of the amorphous phase, and the structure of the nanocrystals. The last method allows determining atomic arrangement in amorphous structure, strain in crystalline materials with a high spatial resolution, etc. The development of the nanobeam electron diffraction with a coherent electron beam lesser than 1 nm in diameter has made it possible to obtain two-dimensional diffraction patterns from a nanoscale region to detect local atomic structure. Combination of the nanobeam diffraction experimental method with *ab initio* molecular dynamics simulation allows obtaining and developing new knowledge about amorphous structure [35, 36]. The newly developed Cs-corrected TEM technique offers a great advantage to probe the local atomic structure of disordered metallic glasses since it allows achieving a coherent electron beam as small as  $\sim 3$  Å in diameter, which cannot be obtained before by conventional TEM [37].

In studying the structure of the amorphous phase, indirect methods may be used such as the measurement of certain properties, whose changes reflect changes in the structure. For example, structure change can be fixed by measuring the temperature dependence of the magnetic properties. Thus, during heating of the ferromagnetic  $\text{Fe}_{27}\text{Ni}_{63}\text{P}_{14}\text{B}_6$  amorphous alloy, there was an increase in the Curie temperature [38]. Since the Curie temperature is determined by the nearest environment of atoms, its change, of course, indicates a change in the structure of amorphous phase. In [39], it was shown that after the heat treatment, the amorphous Fe-P-B alloy is not uniform, and it is characterized by two different Curie temperatures. Numerous studies of amorphous alloys by Mössbauer spectroscopy showed that depending on the conditions of heat treatment, the parameters of the Mössbauer spectra may vary considerably [40]. Application of NMR spectroscopy revealed that the temperature change can lead to changing type of short-range order in the amorphous phase [41].

### 3.2. Structure models

A number of researchers have tried to describe the structure of the amorphous phase in metallic glasses by different models. The first model was the model of a chaotic close packing of hard spheres [42], which allowed successfully describing the distribution function of the atoms in the amorphous structure. Model chaotic close packing of hard spheres was initially designed to one-component systems, and later was adapted to the binary system [43]. Later this model has been improved by the introduction of interatomic potentials (soft-sphere model), which allowed to build atomic pair distribution function [44] with the more realistic values of the position and intensity of the main part and the shoulder of the second maximum of the distribution function. The next step in the modeling of the structure of metallic glasses was attempts to build a structure made up not of individual atoms and of coordination polyhedra [45, 46]. Another group of models of the metallic glass structure is based on the idea that elements of the crystal structure retained in liquid and amorphous alloys [47]. The review [33] lists all the main issues to date models of the structure of amorphous alloys: model of chaotic packing of hard spheres; model of polyhedra packing; the stereochemical model, model of efficient packing of quasi-equivalence clusters [47–51] and the model of middle-range order or fractal packaging [52].

### 3.3. Heterogeneities in amorphous structure

Any approach to the description of the amorphous structure suggests that it is a homogeneous isotropic structure. In fact, it was turned out that the structure of the amorphous phase in alloys cannot always be uniform and isotropic. **Figure 1** shows a typical X-ray scattering curve of amorphous alloy. The figure shows intensive first diffuse peak, determining the shortest distance between atoms and the subsequent weak halo. A feature of the amorphous phase in the metal-metalloid alloys is significantly weaker scattering from metalloid atoms compared to metallic atoms (e.g., an amorphous phase in alloys of Fe-B); therefore, the scattering is determined primarily by the metal atom. Other situation occurs in the case when the amorphous phase contains two or more metals with comparable scattering amplitude (e.g., Fe-Zr). In such systems, the appearance of inhomogeneity areas is much more pronounced, since the formation of regions with different chemical compositions (e.g., enriched in iron or zirconium) [53] leads to the appearance of at least two types of the shortest distances between atoms, which naturally affect the X-ray diffraction pattern. Such changes have been found in a number of systems [54–60].

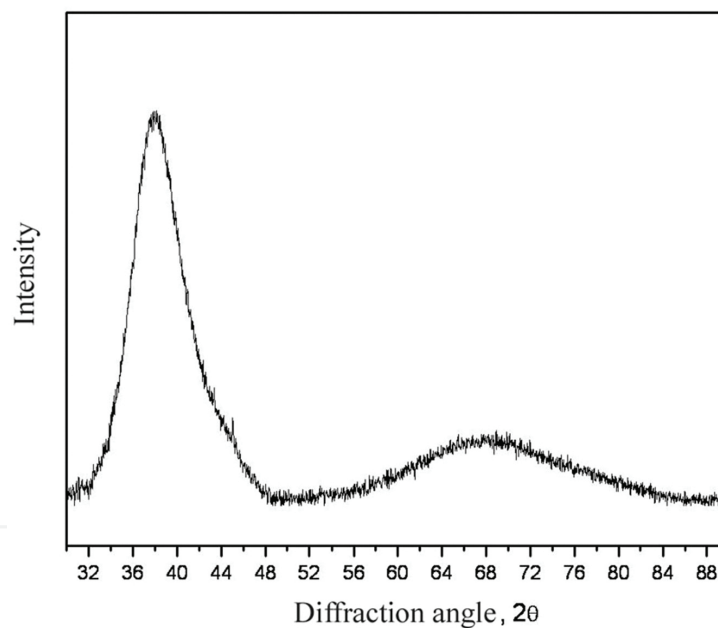


**Figure 1.** X-ray diffraction pattern of amorphous alloy.

It should be noted that X-ray diffraction pattern of the sample shown in **Figure 1** does not indicate that the amorphous phase is uniform. The appearance of a shoulder or a second peak occurs when the radii of the coordination spheres in different regions of the sample are different. If the areas, even with different chemical compositions, have the same radius of the first coordination sphere, no features on the X-ray diffraction patterns will be seen.

Heterogeneities in the structure of the amorphous phase were observed not only in as-prepared state. In some cases, the appearance of heterogeneities in the structure was found after various external influences: heat, irradiation, and others [61–65]. A lot of information about heteroge-

neities in the amorphous phase was obtained using the method of small-angle X-ray scattering [66–70]. It is interesting to note that the occurrence of heterogeneities may be related to the composition of the amorphous phase [56]. The impact of external influences on the structure of the amorphous phase will be discussed in more detail in Section 6.

#### 4. Structure relaxation

Nucleation and growth of the crystals are suppressed at rapid cooling of the melt, and below the melting point metastable supercooled liquid is formed. With the temperature decrease the viscosity increases and the diffusion slows down, that is why at room temperature the solidified structure has the same atomic arrangement as it is in the melt prior to cooling. This non-equilibrium state is usually called the glass and the temperature at which solidification occurs—a glass transition temperature  $T_g$ . The  $T_g$  is generally defined as the temperature when the viscosity of the supercooled liquid reaches  $10^{12}$  poises [6]. At the glass transition temperature, a lot of properties change drastically: specific heat, the temperature dependence of the specific volume, enthalpy, and others. Since amorphous alloys are obtained by melt quenching with cooling rates of  $10^6$ – $10^9$  K/s, the structure of the amorphous phase after quenching is non-equilibrium. When heated, the amorphous phase relaxes to an equilibrium state. There is reversible and irreversible structural relaxation. The volume, viscosity, diffusion mobility, and embrittlement change irreversibly during relaxation; induced magnetic anisotropy may change reversibly, a decrease of internal stress (e.g., during annealing), Young's modulus, specific heat, coercive force, Curie temperature, the internal friction can vary and reversibly and irreversibly depending on the alloy composition [71, 72]. Relaxation processes were widely studied [73–81].

#### 5. Deformation and mechanical properties of amorphous alloys

The main features of the deformation of metallic glasses are a great amount of elastic deformation (up to 4% in the bulk amorphous alloys), high strength, and fracture toughness [7]. Elementary carriers of deformation in metallic glasses are groups of atoms [82]. In contrast to crystalline materials in which the acts of deformation can be estimated from the behavior of dislocations by transmission electron microscopy, it is virtually impossible to observe such a process in metallic glasses. It is usually assumed that the reason for plastic flow and fracture is the formation of shear bands that develop over time. Deformation of metallic glasses proceeds differently in the two different modes of loading and temperature. At high stresses and relatively low temperatures, deformation occurs heterogeneously and it is much localized. As a result, narrow shear bands formed, the orientation of the shear bands is close to the orientation of the maximum shear stress [83, 84]. The time of formation of shear band is estimated as  $\tau < 3$  ms. Shear bands and slip steps were observed for a number of amorphous alloys. Shear bands are oriented at an angle of  $55 \pm 5^\circ$  to the direction of deformation. Upon annealing, the difference in the structure of shear bands and the surrounding matrix can fully

or partially disappear. At low stresses, the deformation is carried out by a homogeneous creep mechanism.

It is important to note one more feature of the deformation of metallic glasses. When stress is applied initially, in accordance with Hooke's law, elastic deformation occurs in which the elongation linearly depends on the stress. At higher loads, this dependence deviates from the linear law. If so-called mechanical hysteresis loop is observed after the load removing, and the sample does not return to its original shape, one talks about the inelastic deformation of the material. The energy corresponding to the area of the loop, connected with the displacement of atoms in a stable position. The quantity of such displacement in the amorphous alloys is generally about an order of magnitude greater than in crystalline alloys. It is believed that the inelasticity of amorphous alloys is related to the free volume in their structure: if the free space is small, the inelastic deformation is also small. A further plastic deformation of amorphous alloys occurs by the formation and propagation of shear bands. It has been found that the velocity of propagation of shear bands does not depend on the strain rate in the range  $2 \times 10^{-4}$ – $10^{-2} \text{ s}^{-1}$  [84]. For such different metallic glasses as ductile  $\text{Pd}_{40}\text{Ni}_{40}\text{P}_{20}$  alloy (value of the plastic strain of about 3%) and fragile  $\text{Mg}_{58}\text{Cu}_{31}\text{Y}_6\text{Nd}_5$  (value of plastic deformation of 0%), the average velocity of propagation of shear bands varies slightly and is 317 and 366  $\mu\text{m/s}$ , respectively [85].

Another feature of plastic deformation of amorphous alloys is the increase in the concentration of free volume in the shear bands, that is, increase in the average distance between the atoms. In general, the features of the shear band structure and, in particular, the reasons for the accelerated mass transfer in these areas are being actively discussed recently. A number of studies assumed that the severe plastic deformation leads to temperature increase up to the melting of the material in shear bands [86–87]. According to another view, shear bands are regions with a disordered amorphous structure of reduced density, so that the diffusion mass transfer in these areas can be facilitated. Probably, mass transfer processes depend both on the temperature rise and on the less dense structure, but these issues are still subject to a more detailed study.

The mechanical properties of amorphous alloys have aroused great interest from the moment when the metallic glasses were first obtained as a ribbon, and it was possible to carry out systematic research. One of the most complete early reviews devoted to the study of the mechanical properties was K. Pampillo's review [83]. Metallic glasses are high-strength materials, some of them can be cut, rolled, and even stamp, and it makes metallic glass attractive for technical applications [88–91]. The properties of metallic glasses are highly dependent on the prehistory of the samples and their chemical composition. Since metallic glasses contain fluctuations, atomic structure may vary slightly from place to place. Structural heterogeneities inevitably lead to irregularities in mechanical properties. Areas with less local viscosity are less stable and can be advantageous in some places of localization of inelastic deformation. These areas are places that facilitated the formation of shear bands [92–94]. Johnson and Samwer [95] derived a universal dependence of the yield strength on the temperature  $(T/T_g)^{2/3}$ . A number of studies suggest that this relationship may be more complicated [96, 97], but the overall trend has been maintained in different systems.

## 6. Effect of heat treatment and deformation on amorphous structure

### 6.1. Effect of heat treatment

When heated, amorphous alloys crystallize, but the crystallization is often preceded by separation of the amorphous phase into regions of different chemical compositions and different short-range order, that is, the formation of two or more amorphous phases. These phases do not separate with sharp interface, and the transformation may exhibit spinodal decomposition characteristics [54, 61]. Changes in the structure of the amorphous phase during annealing were studied for the alloys of various compositions. **Figure 2** presents the X-ray diffraction pattern of  $\text{Al}_{87}\text{Ni}_8\text{La}_5$  sample annealed at  $150^\circ\text{C}$  [98]. After annealing, the samples were amorphous. The structure of the amorphous phase was found to change during annealing, which is revealed in the change of the diffuse maximum in the X-ray diffraction patterns. The first diffuse maximum in the X-ray diffraction pattern of the as-prepared amorphous ribbon was symmetrical, and after annealing it shows a shoulder on the large-angle side, the degree of the maximum distortion increasing with annealing time. **Figure 2** presents the X-ray diffraction pattern of the sample annealed for 25 h (first diffuse peak region). It is seen that subsequent to heat treatment the diffuse maximum is a superposition of two maxima. The positions of the scattering maxima are known to determine the radius of the first coordination sphere  $R_1$ ,

$$R_1 = 7.73 / (S_1)_{\max} = 14.06 / (S_2)_{\max} = 20.46 / (S_3)_{\max} \quad (1)$$

where  $(S_1)_{\max} = 4\pi(\sin\theta / \lambda)$  is the wave vector corresponding to the first (second, third...) maximum of the intensity curve,  $\theta$  the scattering angle, and  $\lambda$  the radiation wavelength [25]. Thus, the two diffuse maxima point to the presence of amorphous matrix regions with different radii of the first coordination sphere. The difference in the angular positions of the diffuse maxima is indicative of the formation of amorphous regions with different chemical compositions of the two amorphous phases. The maximum located at the smaller angles corresponds to the amorphous phase with a large radius of the first coordination sphere (or the largest interatomic distance in the amorphous phase). Since in the system in question the largest atoms are those of lanthanum (radii  $R_{\text{Ni}} = 0.124$  nm,  $R_{\text{Al}} = 0.143$  nm,  $R_{\text{La}} = 0.188$  nm), the amorphous phase is lanthanum-enriched. Thus, the isothermal annealing of amorphous  $\text{Al}_{87}\text{Ni}_8\text{La}_5$  alloy leads to decomposition of the amorphous phase: formation of regions of different chemical compositions and with different types of short-range order.

Similar results were obtained in studies of the effect of prolonged low-temperature annealing on the structure of amorphous Fe-Zr alloy [53]. The annealing of  $\text{Fe}_{90}\text{Zr}_{10}$  sample results in a shoulder on the smaller angle side of the first maximum in the X-ray diffraction pattern: the isothermal annealing leads to amorphous phase decomposition and formation of at least two new amorphous phases with different component concentrations. Such a structural change was also mentioned by the authors of [97] in the studies of metallic Fe-Zr glass by the methods

of anomalous X-ray scattering, nuclear gamma resonance spectroscopy, and magnetic property measurement.

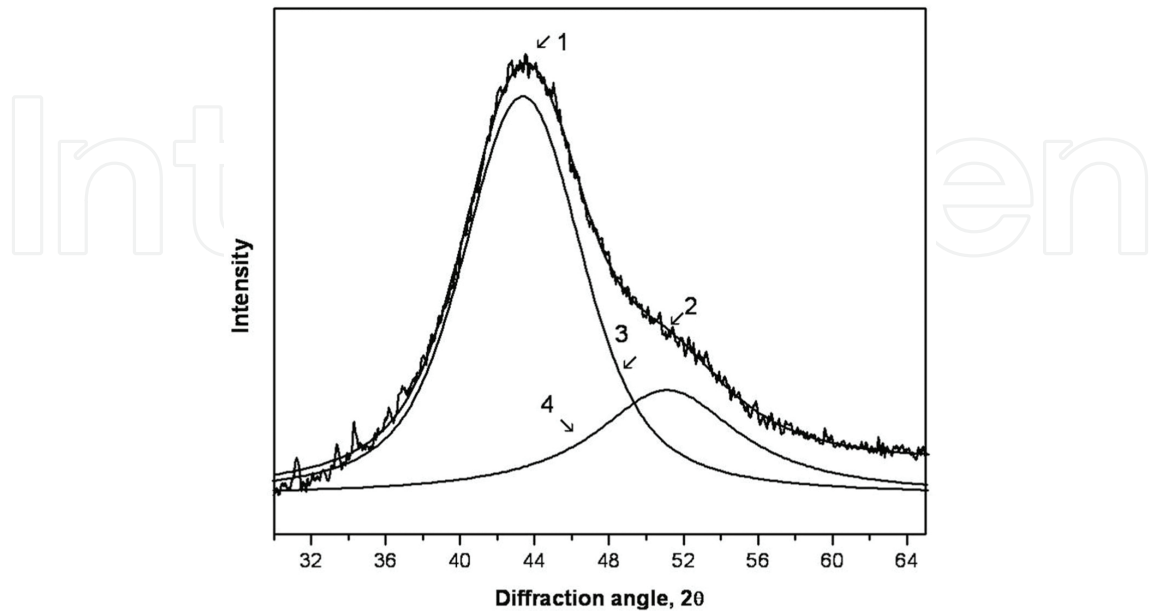


**Figure 2.** X-ray diffraction pattern of as-prepared amorphous  $\text{Al}_{87}\text{Ni}_8\text{La}_5$  alloy (a) and sample annealed at  $1500^\circ\text{C}$  for 25 h (b); 1 denotes the experimental spectrum, 2 the summary curve, 3 and 4 lines the diffusion halos from the first and second amorphous phases.

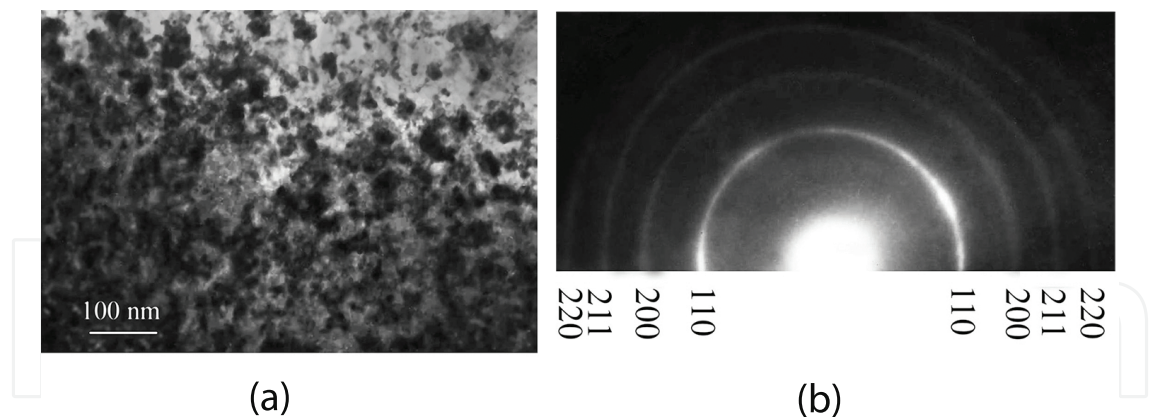


**Figure 3.** Bright field image (a) and electron diffraction pattern (b) of the sample annealed at  $100^\circ\text{C}$  for 6850 h.

**Figure 3a** presents the alloy structure after annealing at  $100^\circ\text{C}$  for 6850 h, and **Figure 3b** presents the corresponding electron diffraction pattern. After this annealing, the sample contains 10–30 nm size crystals. The nanocrystals have non-sharp boundaries in the transmission electron microscopy images. The structure is distinguished by diffuse grain boundaries in the microstructure image and persisting blurred rings in the microdiffraction pattern. Such diffusivity cannot be explained by the small grain size since the diffraction patterns of usual

nanostructures with crystal sizes of 5–10 nm exhibit much more pronounced ring reflections [99]. With increasing annealing time, the structure becomes more distinct and the boundaries between nanocrystals become sharper, and rings in the electron diffraction patterns begin to split. **Figure 4** shows an electron diffraction pattern exhibiting splitting of ring reflection, its more pronounced areas indicated by arrows. It is important to note that these changes in structure occur without appreciable change in scale—the size of nanocrystals is not appreciably changed. The electron diffraction and X-ray diffraction patterns enabled to establish that two solid solutions of Zr in Fe form in the sample, their lattices having close but different parameters and, naturally, different component ratios. The above characteristic features of transformation indicate a progressive and continuous transition from single-phase amorphous structure, then to crystalline structure with diffuse grain boundaries, and, finally, to fully crystalline structure with a constant size the regions of composition changes, point to the spinodal nature of transformation.

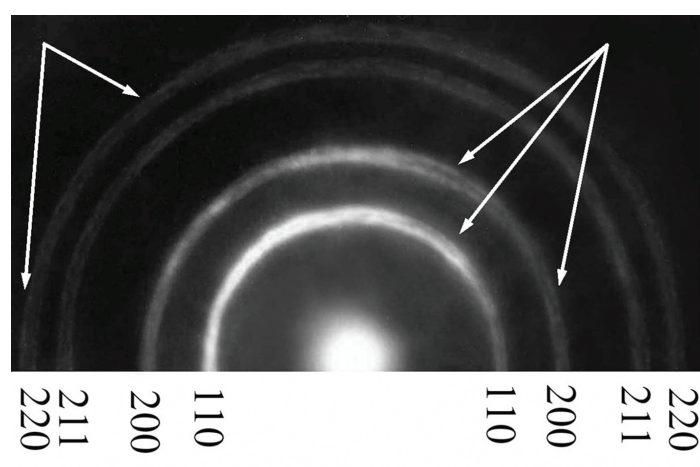


**Figure 4.** Electron diffraction pattern of the sample annealed at 100°C for 7000 h.

Evolution of the amorphous phase depends on temperature. As it was mentioned above, heating and annealing of the metallic glasses can be carried out in two different temperature ranges: above and below the glass transition temperature. Above the glass transition temperature, the amorphous phase is in a supercooled liquid state, below glass transition temperature it is in fact the amorphous state. It is known that when passing through the glass transition temperature  $T_g$ , material properties change sharply (viscosity, enthalpy, heat capacity, specific volume, and others.). This leads to significant differences in the process of diffusive mass transfer in these temperature ranges, and in turn, to changes in the structure. For comparison, let us consider the changes in the structure of the same alloy that occur above and below the glass transition temperature in the two nickel-based glasses: Ni-Mo-P and Ni-Mo-B.

1. *Amorphous Ni<sub>70</sub>Mo<sub>10</sub>P<sub>20</sub> alloy.* The glass transition temperature ( $T_g = 430^\circ\text{C}$  for a heating rate of 20K/min) of the alloy is below the crystallization temperature ( $T_x = 457^\circ\text{C}$ ) [100]. This allows to investigate the changes in the structure both in the supercooled liquid state (above  $T_g$ ) and in the amorphous state (below  $T_g$ ). Heating above the glass transition

temperature leads to a noticeable change in the structure of the amorphous phase. **Figures 5** and **6** show the TEM images of the as-prepared sample (**Figure 5**) and annealed above  $T_g$  sample (**Figure 6**) [100]. Under the same conditions of preparation of electron microscopy foils, in the annealed sample, in contrast to the original, there is a pronounced spotted contrast. **Figure 7** shows the X-ray diffraction patterns of as-prepared and annealed above  $T_g$  samples. After annealing, the shape of diffuse maximum distorted. When analyzing the structure of the amorphous alloy by micro-micro-diffraction method it has been found that the scattering vector corresponding to the maximum intensity of diffuse halo of an amorphous phase varies from one area to another along the sample. Observed area of spotted contrast and matrix is described by the different scattering vectors, indicating that the difference in short-range order in the light and dark areas. With further heating, the crystallization begins in places that appear lighter in the images. In these places, crystals of Ni(Mo) FCC solid solution form; the size of the crystals is 20–30 nm, and crystals are in direct contact with each other (**Figure 8**). If the heat treatment was carried out below the glass transition temperature, changes in the structure of amorphous phase were not observed. The structure of the sample annealed at 400°C for 1 hour (below  $T_g$ ) contains the amorphous phase and crystalline eutectic colonies. Thus, the processes leading to separation of amorphous phase occur at the temperatures above  $T_g$ ; above and below the glass transition temperature, amorphous structure varies differently, later leading to the formation of different crystal structures and, of course, different physical properties.

2. *Amorphous Ni<sub>70</sub>Mo<sub>10</sub>B<sub>20</sub> alloy* [101]. In this alloy, the glass transition temperature is also below the crystallization temperature. Upon heating the amorphous alloy above the glass transition temperature, the X-ray diffraction pattern also changes due to the appearance of areas with different chemical compositions. So before the crystallization the amorphous phase is heterogeneous and contains areas with higher and lower molybdenum concentration (and possibly boron). Crystallization of the alloy above the glass transition temperature leads to the formation of three crystalline phases simultaneously: two face-centered crystalline phases and an orthorhombic phase Ni<sub>3</sub>B. FCC phases are Ni and Ni(Mo) solid solution. All three phases form substantially simultaneously. The crystal size is less than 50 nm. **Figures 9** and **10** show the images of Ni (**Figure 9**) and Ni(Mo) solid solution (**Figure 10**) nanocrystals formed above the glass transition temperature. Each nanocrystal is surrounded by the amorphous matrix. Studies of the structure by transmission and high resolution electron microscopy methods showed that the formation of the phases is independently from each other. The formation of each of the crystalline phases occurs in “their” concentration region, that is, the formation of crystalline phases in each concentration region can occur by the polymorphic mechanism without changing the chemical composition or by primary crystallization mechanism with slight change in concentration. These types of the crystallization (primary or polymorphic instead of eutectic crystallization) are due to changes in the amorphous structure before the crystallization which ensures the formation of amorphous regions to “fit” the compositional ordering. Below the glass transition temperature, phase separation is not observed, the crystallization occurs by the eutectic mechanism.

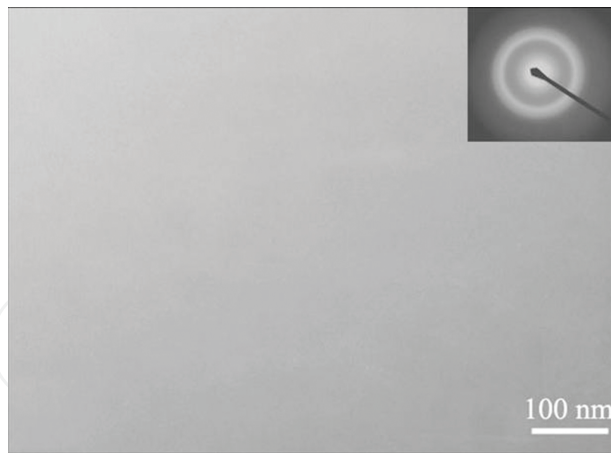


Figure 5. TEM image of the structure of as-prepared amorphous  $\text{Ni}_{70}\text{Mo}_{10}\text{P}_{20}$  alloy.

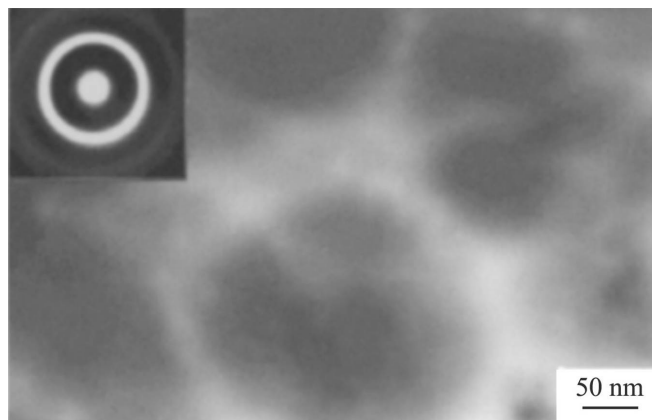


Figure 6. TEM image of the structure of  $\text{Ni}_{70}\text{Mo}_{10}\text{P}_{20}$  alloy annealed above  $T_g$ .

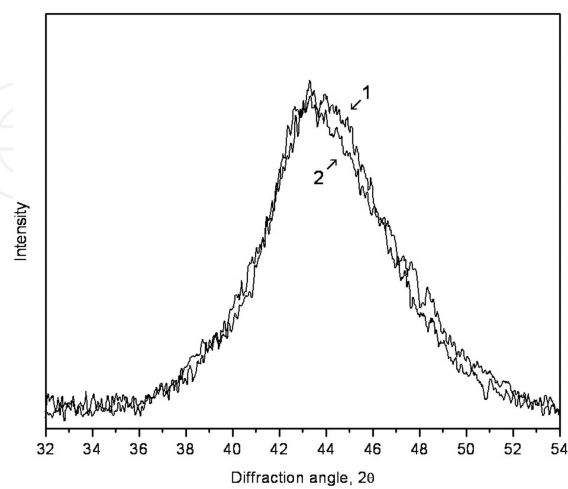
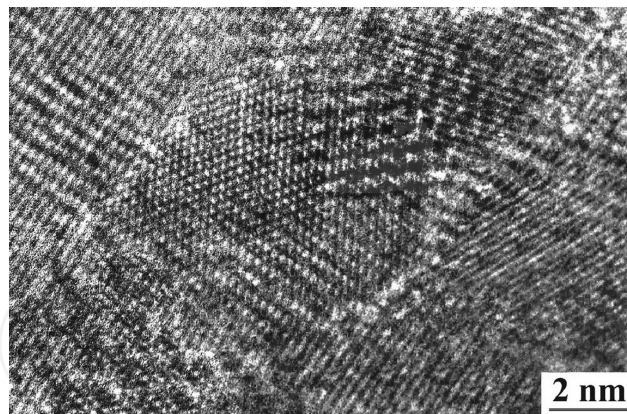
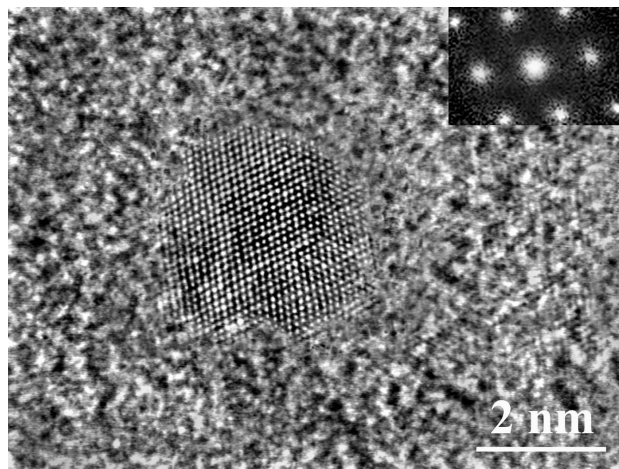


Figure 7. X-ray diffraction patterns of as-prepared and annealed above  $T_g$   $\text{Ni}_{70}\text{Mo}_{10}\text{P}_{20}$  sample.



**Figure 8.** High-resolution electron microscopy image of alloy  $\text{Ni}_{70}\text{Mo}_{10}\text{P}_{20}$  crystallized above  $T_g$ .



**Figure 9.** HREM image of Ni nanocrystals formed above the glass transition temperature.

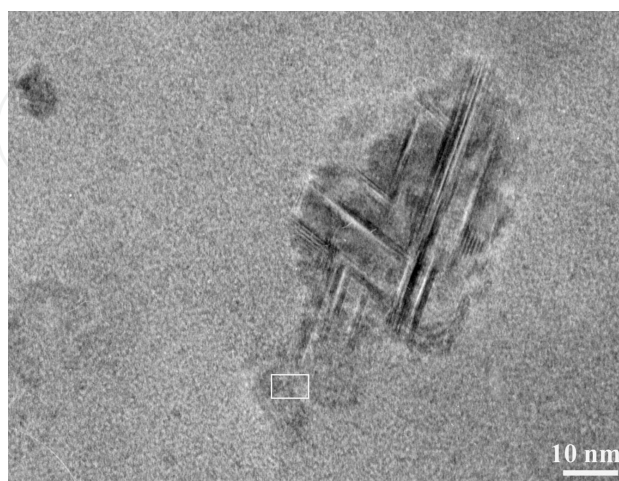


**Figure 10.** HREM image of Ni(Mo) nanocrystals formed above the glass transition temperature.

Thus, structure formed above and below the glass transition temperature varies markedly. It should be noted that the scale of the chemical composition change may be different: it is about (15–20 nanometers) in (Fe-Zr system) [102] or more than 50 nm (Ni-Mo-B system) [99]. This difference is connected with opportunity of implementing a diffusion mass transport in different temperature conditions. As noted above, the results, showing the development of heterogeneities in an amorphous matrix, were obtained using small-angle X-ray scattering method as well [63, 66, 99, 102–104]. Changes in the structure of the amorphous phase do not necessarily have the character of a separation at heat treatment. The type of short-range order can vary with the temperature [41, 105]. Concentration redistribution of the components in the amorphous phase can occur not only before the onset of crystallization. In some cases, the amorphous alloy separation may accompany the first stage of crystallization [99, 106].

## 6.2. Effect of deformation

The structure of amorphous phase can vary considerably, not only by heating but also by deformation. The question of a possible change in the structure under the influence of the deformation came into sight from the very beginning of amorphous alloy research. As was mentioned problems of homogeneous deformation and inhomogeneous flow, the fracture processes, their dependence on the temperature and composition was discussed in [83, 107]. In the last few years, new works were published that confirm the change in the structure of the amorphous phase at different types of influences which do not lead to crystallization [108]. A group of studies on the structure evolution carried out directly in the process of deformation of Zr-based amorphous alloys aroused great interest. The samples were deformed by tension, and synchrotron source was used for structure investigation in-situ. It allowed detecting the structure occurring at the elastic deformation [109–111]. It has been found that in the absence of plastic deformation, the tensile results in a change of the distance between atoms in an amorphous structure, and these changes depend on the orientation of the applied stress. It was shown that the initial symmetric with respect to zero diffuse peak position becomes asymmetric in the process of deformation. The results indicate that the first coordination sphere, characterizing the arrangement of atoms in the amorphous structure, transformed into an ellipsoid in the deformation process. In the study of elastic deformation of  $Zr_{62}Al_8Ni_{13}Cu_{17}$  and  $La_{62}Al_{14}(Cu_{5/6}Ag_{1/6})_{14}Ce_5Ni_5$  metallic glasses the deformation was shown [108] to be indeed an anisotropic. The Zr-based amorphous alloys are brittle, and they practically do not undergo plastic deformation, so only the region of elastic deformation was considered in the above-mentioned paper. At the same time, it would be interesting to determine whether the observed changes in the structure can be stored when the load is removed and whether they exist at plastic deformation. Such studies have been carried out for the amorphous  $Pd_{40}Ni_{40}P_{20}$  alloy [112]. The deformation by multiple rolling was found to cause formation of anisotropic amorphous structure. The distance between atoms along the rolling direction was found to increase at the deformation, whereas it does not change in the perpendicular direction. Changes in the structure during deformation have been observed using a small-angle X-ray scattering method [113, 114].

In addition to the occurrence of the anisotropy in the structure, plastic deformation may lead to separation of the amorphous phase. **Figure 11** shows the X-ray diffraction patterns of amorphous  $\text{Al}_{88}\text{Ni}_2\text{Y}_{10}$  and  $\text{Al}_{88}\text{Ni}_{10}\text{Y}_2$  alloys after deformation by multiple rolling [115]. It is seen that the first diffuse maximum for  $\text{Al}_{88}\text{Ni}_{10}\text{Y}_2$  alloy is asymmetric and, as in the case of heat treatment, it is a superposition of at least two maxima. Note that changing the structure under the influence of plastic deformation depends on the alloy composition. It is evident that the first diffuse maximum from the  $\text{Al}_{88}\text{Ni}_{10}\text{Y}_2$  sample (curve 1 in the X-ray diffraction pattern) is asymmetric and, obviously, it is a superposition of at least two maxima. Two amorphous halos indicate the appearance of regions, which differ in composition. So, rolling of the  $\text{Al}_{88}\text{Ni}_{10}\text{Y}_2$  alloy leads to separation of the amorphous phase into regions with different chemical compositions. Deformation of  $\text{Al}_{88}\text{Ni}_2\text{Y}_{10}$  alloy (curve 2, **Figure 11**) leads to formation of a small amount of nanocrystals.

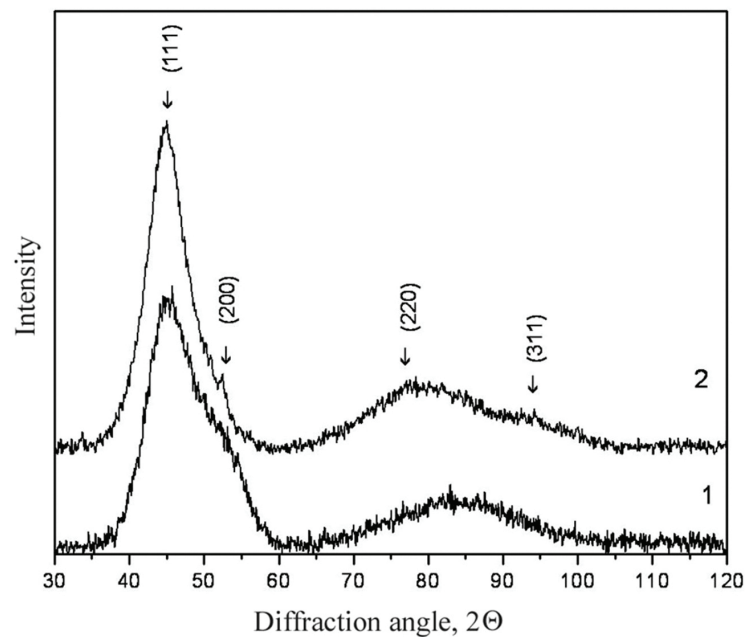


**Figure 11.** X-ray diffraction patterns of deformed  $\text{Al}_{88}\text{Ni}_{10}\text{Y}_2$  (1) and  $\text{Al}_{88}\text{Ni}_2\text{Y}_{10}$  (2) alloys.

## 7. Property change during amorphous phase evolution

The physical properties of amorphous alloys are very sensitive to structure evolution; they depend on external influences. Amorphous phase is not thermally stable, so the subsequent annealing, not leading to crystallization, causes the structure change:

- *The microhardness change.* Changes in the structure during annealing are accompanied by changes in microhardness of amorphous phase. For example, microhardness marked increases at low-temperature annealing of amorphous  $\text{Fe}_{80}\text{B}_{20}$  alloy [116]. Since the microhardness of the material characterizes the strength of the bonds between atoms in

the structure, change of microhardness shows evident amorphous structure evolution. The increase of the microhardness during annealing is obviously caused by both decreasing free volume and ordering processes.

- *The Curie temperature change.* Study of the amorphous  $\text{Fe}_{27}\text{Ni}_{63}\text{P}_{14}\text{B}_6$  alloy [38] showed rising Curie temperature at heating in the temperature range below the crystallization temperature. Later, these changes were observed in a number of other alloys [39, 117]. Heat treatment of amorphous Fe-B-P alloy was found to lead to separation of the amorphous phase into region differing in composition and/or short-range order, which can be characterized by different Curie temperatures. The changes of the properties with heat treatment may be reversible [118, 119].
- *Changes in plasticity.* The ductility of amorphous alloy decreases during heating. This decrease can start at a sufficiently low temperature compared to the temperature of crystallization depending on the chemical composition. The embrittlement of amorphous alloys was first detected in the  $\text{Fe}_{40}\text{Ni}_{40}\text{P}_{14}\text{B}$  alloy, and it was believed that it is caused by the presence of phosphorus, since it was found that the fracture surface is enriched with phosphorus [119]. However, Masumoto et al. [29] showed that the Fe-Si-B alloys without phosphorus are also fragile.

## 8. Crystallization processes

Since amorphous state is metastable, the amorphous alloys transform into a more stable crystalline state at heating. In most cases, the crystallization of the amorphous phase occurs by the mechanism of nucleation and growth. The most detailed crystallization reactions were studied by U. Koester in Bochum University [120]. The transition of the amorphous phase into crystalline phases depending upon the alloy composition can occur by one of the following reactions.

- primary (or preferential) crystallization;
- eutectic crystallization;
- polymorphic crystallization.

When the primary crystallization occurs, concentration gradient arises in front of the growing crystal. The growth rate decreases with time because the reaction involves the atoms diffusing on the long distances. It has been found that the spherical radius  $R$  of the growing crystal parabolically depends on the annealing time  $t$  in many metallic glasses which crystallize in the primary crystallization reaction [120, 121]. This means that the crystal growth is controlled by bulk diffusion,

$$R = \alpha \sqrt{(Dt)} \quad (2)$$

where  $\alpha$ —dimensionless parameter depending on the composition at the interface particle/matrix, and  $D$ —the coefficient of volume diffusion.

The polymorphic and eutectic crystallization mechanisms are studied in [122, 123].

The crystal nucleation can be homogeneous and heterogeneous, in the last case the formation of crystals will be facilitated on the surfaces or so-called “frozen” crystallization centers [124, 125]. The ratio of nucleation and growth rates is a very important factor in the formation of structure. At low nucleation rate and high growth rate, small number of crystals forms and they can grow to considerable size. In the case of high nucleation rate and a small growth rate, very large number of crystals forms in the amorphous matrix.

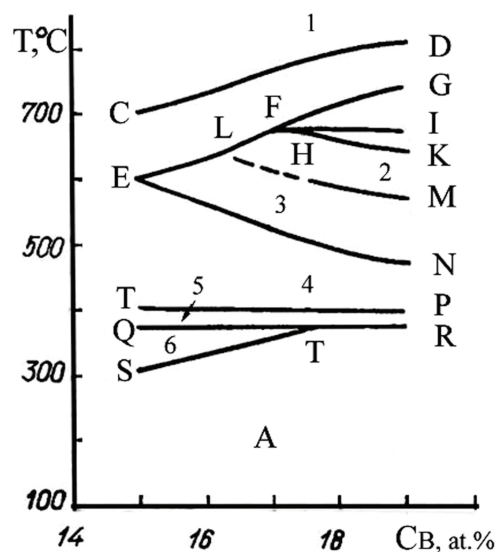


**Figure 12.** A diagram of phase transformation: I -  $\alpha$ -Fe +  $\text{Fe}_2\text{B}$ , II -  $\alpha$ -Fe +  $\text{Fe}_3\text{B}(\text{P}_{42}/\text{n})$ , III -  $\alpha$ -Fe +  $\text{Fe}_3\text{B}(\text{P}_{42}/\text{n})$  +  $\text{Fe}_3\text{B}(\text{I}^-4)$ , IV -  $\alpha$ -Fe +  $\text{Fe}_3\text{B}(\text{I}^-4)$ , V - A +  $\alpha$ -Fe +  $\text{Fe}_3\text{B}(\text{I}^-4)$ , VI - A +  $\alpha$ -Fe, IHK -  $\alpha$ -Fe +  $\text{Fe}_3\text{B}(\text{P}_{42}/\text{n})$  +  $\text{Fe}_3\text{B}(\text{P})$ , GFI -  $\alpha$ -Fe +  $\text{Fe}_3\text{B}(\text{P})$  +  $\text{Fe}_3\text{B}(\text{Pnma})$ .

In addition to the above reaction of nucleation and growth crystallization, the mechanism of spinodal decomposition may occur at the metallic glass crystallization [126]. The possibility of such a separation in metallic glasses was discussed in a number of papers [127, 128–130]. The crystal structure formed during the crystallization of the amorphous phase can vary significantly in phase composition, morphology, crystal size, mutual arrangement of structural components [131]. In the last decades, much attention has been paid to nanocrystalline structure. The nanocrystalline structure in most cases is formed by the primary crystallization reaction. The Fe-Cu-Nb-Si-B alloy, called Finemet, was the first alloy obtained in the nanocrystalline structure [132].

An important feature of the crystallization of metallic glasses is the fact that in most cases, crystallization begins with the formation of metastable phases. As an example, crystallization of most extensively studied Fe-B metal glasses may be considered [133–135]. In accordance with the phase diagram of the system [106], the crystallization of compositions close to the eutectic must occur by  $\alpha$ -Fe and tetragonal  $\text{Fe}_2\text{B}$  boride formation. However, the crystallization

leads to the formation of  $\alpha$ -Fe is formed of tetragonal  $\text{Fe}_3\text{B}$  boride. This boride may form different structures (crystalline lattice of different space group), which undergoes several changes before equilibrium phase turns into  $\text{Fe}_2\text{B}$  at heating or annealing. Specific features of metastable  $\text{Fe}_3\text{B}$  boride were studied in a lot of work [93, 134, 136, 137]. **Figure 12** illustrates a diagram of Fe-B metallic glass transformation; the regions of existence of different borides are shown.

Another example is the crystallization of the amorphous  $\text{Ni}_{34}\text{Zr}_{66}$  alloy [138]. This alloy belongs to a small group of metallic glasses, which, in principle, can crystallize by polymorphic crystallization mechanism with formation of equilibrium  $\text{NiZr}_2$  crystalline phase (tetragonal lattice of  $I4/mcm$  space group). However,  $\text{NiZr}_2$  phase was not observed at the crystallization; a metastable phase with an orthorhombic lattice was formed. In contrast to the equilibrium phase, the structure of the metastable phase has a lower symmetry.

The formation of metastable phases at the crystallization of the amorphous phase is often observed for multi-component systems. Crystallization of multi-component Zr-based alloys and changes in the structure and properties at treatment were examined for the alloys of different composition [139–145]. The crystalline structure forming at amorphous phase decomposition is strongly dependent on the chemical composition. For example, the amorphous  $\text{Zr}_{65}\text{Cu}_{17.5}\text{Ni}_{10}\text{Al}_{7.5}$  alloy crystallizes with simultaneous formation of three phases:  $\text{NiZr}_2$ -type phase with cubic lattice,  $\text{NiZr}_2$  tetragonal phase and a metastable hexagonal phase, the crystals of all phases are randomly distributed in the amorphous matrix. When reducing the zirconium concentration, the phase composition varies. At the first stage of crystallization of the amorphous  $\text{Zr}_{50}\text{Ti}_{16}\text{Cu}_{15}\text{Ni}_{19}$  alloy, three phases are formed, two of them are crystalline and the third phase is quasicrystalline. Quasicrystalline phase was observed in a number of crystallized metallic glasses of different composition [145–149].

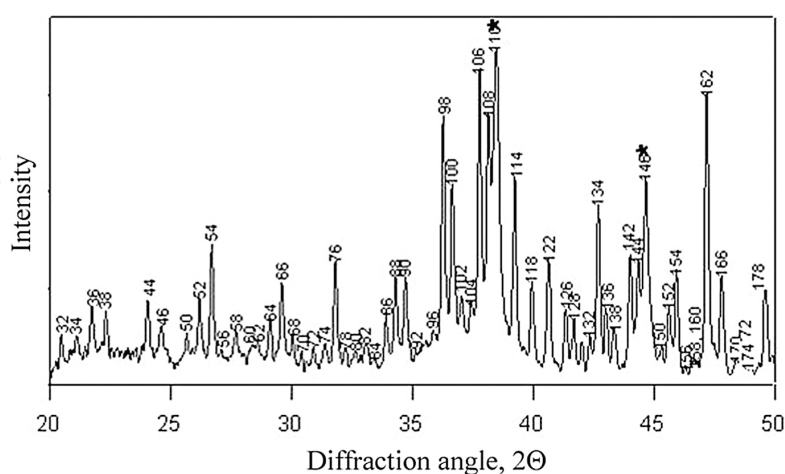


**Figure 13.** Part of X-ray diffraction pattern of  $\text{Al}_{85}\text{Ni}_{10}\text{Ce}_5$  after the first stage of crystallization.

One more example: decomposition of the amorphous phase in the  $\text{Al}_{85}\text{Ni}_{10}\text{Ce}_5$  metallic glass [150, 151]. The alloy crystallization begins with the formation of metastable phase. **Figure 13**

shows the X-ray diffraction pattern of the alloy after the first crystallization stage. After finishing the first stage, the sample is predominantly crystalline, but it retains a certain amount of amorphous phase. All the observed diffraction lines correspond to one crystalline phase with a body-centered cubic lattice. **Figure 13** shows only a part of the investigated spectrum; the sum of the squares of the indices  $\Sigma = h^2 + k^2 + l^2$  is shown near each line. Usually the pure aluminum crystals form at the first stage of crystallization of Al-Ni-RE (RE = Y, Yb, Ce) alloys (nickel and rare earth components do not dissolve in FCC-Al). Since the ratio of the cell parameters of metastable phase and fcc-Al  $a_{MS}/a_{Al} = 6.05$ , it was assumed that the metastable phase forms in a situation when the concentration redistribution of the components of the “uniform” amorphous phase has no time to occur. As a result, metastable solid solution of the alloy components in Al lattice form, it has a much larger lattice parameter, wherein the concentration of nickel and cerium is noticeably greater than their equilibrium solubility in the Al lattice.

Changes in the structure during the phase transformation from an amorphous phase to the crystalline equilibrium phase are accompanied by a change in the physical properties [118, 152]. Structure formed at the crystallization of metallic glasses varies also during deformation or pressure increase [153–155], icosahedral quasicrystals have been found at the crystallization of a number of metallic glasses [155–158].

## 9. Nanocrystalline structure formation

Under certain conditions, crystallization leads to the formation of a nanocrystalline structure. Nanocrystalline materials may be single-phase and multiphase polycrystalline samples with a grain size of up to 100 nm (at least in one direction). Owing to the extremely small size of the grain, the structure of nanocrystalline materials is characterized by a large volume fraction of grain boundaries and interfaces, which can largely determine a variety of physical and chemical properties of the material. Indeed, it has been found that many properties of nanocrystalline material are fundamentally different from those of conventional polycrystalline and amorphous alloys [159, 160]. For instance, nanocrystalline materials may have high strength and hardness, good ductility and toughness, reduced elastic modules, higher diffusion rates, large heat capacity and thermal expansion coefficient, and higher magnetic properties as compared to conventional materials [161–164]. The nanocrystalline materials not only provide an excellent opportunity to study the nature of structure, properties, and structure/properties correlation of solids down to the nanometer range, but they are also very attractive in terms of possible industrial use of new materials [165]. Changes in the structure and properties of amorphous and amorphous-nanocrystalline materials have been studied in a number of papers [166–169]. Small grain size makes a great development and length of the grain boundaries. The grain volume fraction of the grain boundaries in the total amount of the nanocrystalline particles in the material can be estimated in spherical shape approximation as in [170]:

$$\Delta V / V = [\pi d^3 / 6 - \pi(d - 2\delta)^3 / 6] / (\pi d^3 / 6) \approx 6\delta / d \quad (3)$$

where  $\delta$  is the average thickness of the interface and  $d$  is an average grain diameter [170]. Thus, one can estimate the volume of the grain boundary. For example, when the thickness of the interface  $\delta$  is 3–4 atomic monolayers (0.5–1.5 nm) and the average grain size is 10–20 nm, the fraction of surface layer is about 50%.

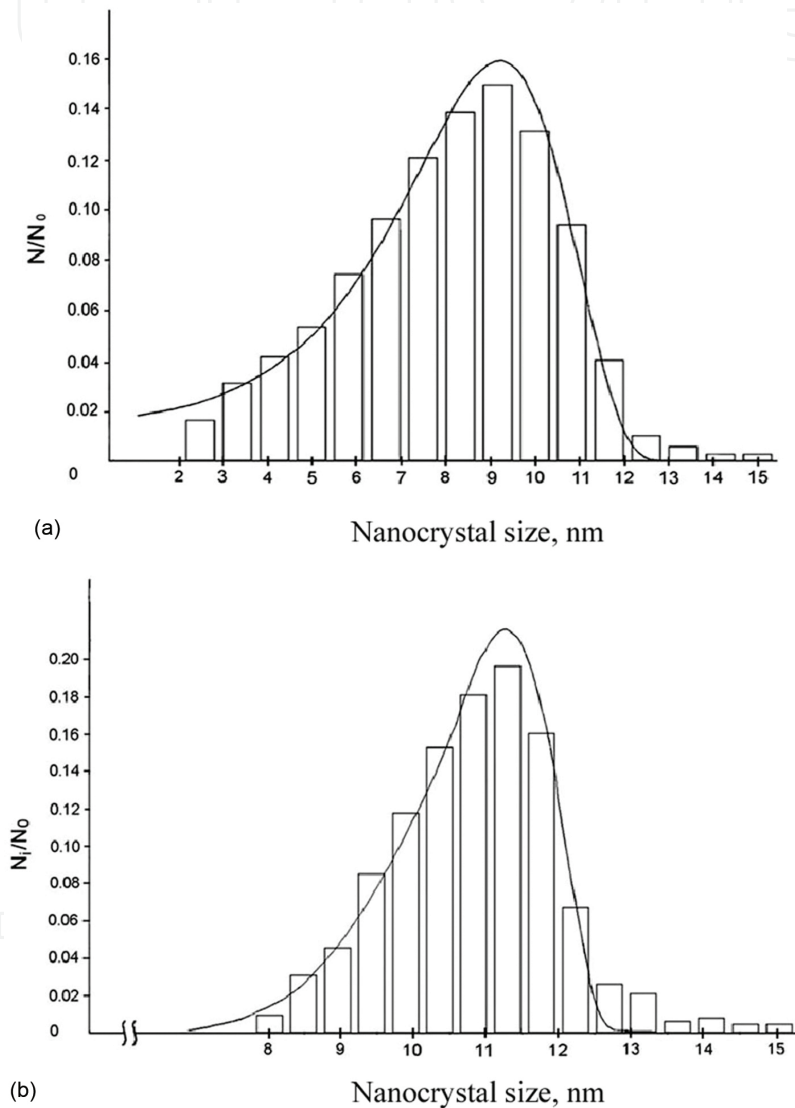


**Figure 14.** The crystal distribution by size after annealing at 473 K for 5 (a) and 15 (b) min: experimental (columns) and calculated (line) data.

Crystallization of amorphous alloys usually takes place under conditions of existence of the large driving forces and low diffusion mobility. These conditions are favorable rather for nucleation and not for crystal growth. Formation and specific features of nanocrystalline structure were studied for different materials [171–175]. Specific nanocrystalline/amorphous

composite structure has excellent magnetic or mechanical properties in a number of alloys [176–178].

To establish the mechanism of nanocrystallization, one can use a method of analysis of crystal size distributions. For example, controlled crystallization of the amorphous  $\text{Al}_{86}\text{Ni}_{11}\text{Yb}_3$  alloy [179] was found to lead to the formation of nanocrystalline structure with nanocrystal size of 5–12 nm. The nanocrystals are formed according to the mechanism of the non-stationary heterogeneous nucleation and from frozen-in crystal nuclei. For the conclusion of the nucleation mechanism, the distributions of nanocrystals by size were plotted for different durations of isothermal annealing; the distributions were analyzed. The size distributions obtained upon treatment for 5 and 15 min are depicted in **Figure 14a** and **b**, respectively. It is apparent that the heterogeneous nucleation with a latent period proceeds in our case. This is confirmed by the following facts. (1) Small-sized crystals are absent in the distribution obtained upon treatment for 15 min. (2) A sharply descending portion in the small-size range is observed in the distribution at a treatment time of 5 min, which is impossible in the case of homogeneous nucleation. (3) The fraction of large-sized particles (the right-hand branch of the distribution) decreases gradually, which is characteristic of the non-stationary rate of nanocrystal nucleation (with the latent period). Therefore, at the very early stage of metallic glass annealing, there exists a certain time interval during which the stationary size distribution of subcritical nuclei (corresponding to the classical theory) is reached.

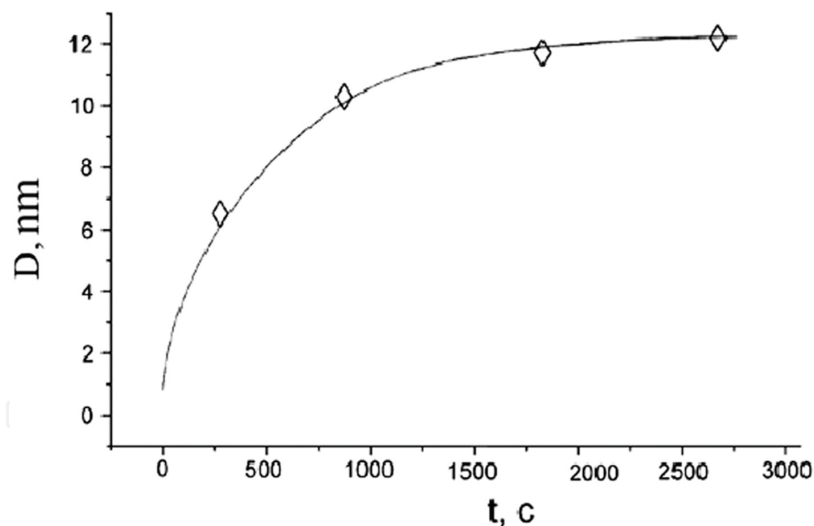


**Figure 15.** The dependence of the average crystal size in the  $\text{Al}_{86}\text{Ni}_{11}\text{Yb}_{31}$  alloy on the annealing time time.

Computer simulations were carried out for heterogeneous nucleation and diffusion controlled growth. The calculated crystal distributions by size for annealed  $\text{Al}_{86}\text{Ni}_{11}\text{Yb}_3$  alloy (473 K for 5 and 15 min) are shown by lines in **Figure 14**; the experimental size distributions are represented by columns. Good agreement with the experimental data was obtained for the following crystallization parameters:  $Q_N = 90 \times 10^3$  J/mol and  $\tau = 150$  s. The effective diffusion coefficient of Ni and Yb in amorphous  $\text{Al}_{86}\text{Ni}_{11}\text{Yb}_3$  alloy is  $1.4 \times 10^{-19}$   $\text{m}^2\text{s}^{-1}$  for 5 min annealing and  $6 \times 10^{-20}$   $\text{m}^2\text{s}^{-1}$  for 15 min annealing. Since the diffusion coefficient of nickel, as a rule, is considerably

larger than that of ytterbium, it is assumed that the nanocrystal growth is limited by the diffusion rate of ytterbium. As seen in **Figure 14**, the calculated and experimental data are very similar. However, the difference between the calculated and experimental distributions is in the presence of a tail of large-sized particles in the experimental histograms. Most likely, the occurrence of large-sized particles can be explained in terms of the presence of a small number of so-called “frozen-in crystal nuclei” in the initial alloy. The formation of crystals from these nuclei is facilitated. As a result, particles begin to grow earlier (prior to the completion of the latent period of attaining the stationary size distribution of subcritical nuclei) and reach larger sizes. **Figure 15** shows the dependence of the average crystal size in the  $\text{Al}_{86}\text{Ni}_{11}\text{Yb}_3$  alloy on the annealing time. The similar results were obtained for the crystallization of amorphous Al-Ni-Y alloys [180]. It has been found that the nanocrystals are nucleated by heterogeneous mechanism in the aluminum-based alloys; and the nucleation begins in the regions depleted in the rare earth component [99, 174]. Specific features of the nanocrystal formation are studied in detail in [180–183].

## 10. Specific features in nanocrystalline structure

Since metallic glasses are often used as the starting material for producing nanostructures, and problem of deformation of the composite amorphous-nanocrystalline material is very important. Naturally, an important question is what component (nanocrystal or amorphous phase) determines the mechanical properties of the material and, in particular, if the nanocrystals can be deformed. Questions of the deformation of nanostructures are discussed in detail in [170]. Usually single unloaded volume unit contains a small amount of induced defects or does not contain them at all. The smaller the size of the nano volume, the smaller the number of induced defects it contains. A critical particle size with a free surface  $d_c$  was assumed to can be estimated if believe that below the probability of the existence of the defect sharply decreases [171, 172]. It was suggested that  $d_c$  is about 10–100 nm. Such estimates have been made for free nanoparticles. It was assumed that I also believe that the mechanisms of plastic deformation and fracture of nanocrystalline materials are determined by the size effect.

In this way, the solution to this problem largely rests on the question whether the nanocrystals contain dislocations, which are carriers of plastic deformation. In the early stages of research, it has been suggested that there is a critical size below which all the crystals are perfect; and the crystals contain stacking faults, twins, etc. when exceeding this size. In fact, at the initial moment when the crystals nucleate and grow in an isotropic amorphous phase, they really are perfect. When the crystal growing, when the volume per one atom in the crystal is differ then the volume per atom in the amorphous phase, there are tension stresses around the crystals. The value of these stresses increases as the crystals grow and conditions for the formation of linear defects arise. Is there, indeed, a certain critical size of crystal separating perfect and imperfect crystals? The answer is quite important in particular for determining the strength and ductility of the material. For example, it was supposed in [170] that such a critical crystallite size determines the boundaries of the regions where mechanisms of dislocation strengthening and plasticity cease to operate.

Specific features of the nanocrystalline structure were studied in detail in [174–178] for Al- and Ni-based alloys. The results showed that the Al nanocrystals and Ni nanocrystals formed in eutectic Ni-Mo-B systems were defect-free. These nanocrystals have equiaxial shape, small size, and they do not contain linear defects. The nanocrystals of Ni (Mo) solid solution in all studied alloys were defect-free at the beginning of crystallization, while the size of the nanocrystals is not more than about 5 nm. However, in the fully formed nanostructure the average size is much larger (20–50 nm), and the nanocrystals contain a significant number of defects. In analyzing the reasons of defect formation in the nanocrystals, two factors: the size factor and the energy of stacking fault formation, were considered. This size factor is associated with the inability to generate dislocations in nanocrystals smaller than 100 Burgers vector (operation conditions of dislocation sources, such as the Frank-Read [184]). It is also obvious that the probability of appearance of defects (e.g., stacking faults) depends on the energy of their formation, and of course, this factor must be taken into account when comparing the degree of perfection of different nanocrystals. In terms of the magnitude of the Burgers vector  $b$ , the average size of the nanocrystals is:

Ni in the alloy with 20 at.% B  $8\text{--}20 b$ ,

Al  $\sim 40\text{--}45 b$

(the Burgers vector is  $b_{\text{Ni}} = a_{\text{Ni}}/2 [110] = 0.250 \text{ nm}$  for Ni nanocrystals and  $b_{\text{Al}} = a_{\text{Al}}/2 [110] = 0.286 \text{ nm}$  for Al nanocrystals).

As was mentioned, when analyzing the degree of nanocrystals perfection in the Al- and Ni-based systems, the influence of the energy of stacking fault formation was considered [174]. The value of the energy of stacking fault formation is  $135 \text{ erg/cm}^2$  for Al and  $240 \text{ erg/cm}^2$  for Ni. However, it is known that the energy of stacking fault formation decreases with increasing electron concentration when doping [185]. For example, stacking fault energy in Cu-Ag alloys decreases  $\sim 10$  times with increasing electron concentration to 20% [186, 187]. Unlike aluminum nanocrystals that are one-component, nickel nanocrystals contain about 17 at.% Mo, which leads to an increase in the electron concentration to about 20%. It is therefore natural to expect a significant reduction (several times) the stacking fault energy. This reduction of the energy of stacking fault formation can explain more perfect structure of Al nanocrystals as compared to Ni(Mo) nanocrystals.

However, what is a predominant reason of defect formation in the nanocrystals (the size factor or the energy of formation of stacking faults) is not clear.

What can cause the formation of defects in the nanocrystals? As shown above, a significant number of defects were observed in nanocrystals of Ni (Mo) solid solution. Since the nucleation and nanocrystal growth occur by the primary mechanism of crystallization, it is natural to expect that the concentration of molybdenum in nickel lattice varies from the center to the periphery of the nanocrystal. It is known that [187, 188] peculiar ordered structure can be formed in the crystals of two-component systems. It can be assumed that the formation of twins in the nanocrystals of Ni(Mo) solid solution can occur in this way, that is, the formation be facilitated due to the uneven distribution of molybdenum atoms in solid solution. Naturally,

formation of stacking faults by this mechanism is not possible in the case of single-component nanocrystals.

It should be noted that the shape of Ni(Mo) nanocrystals with size of 30–50 nm differs from the equilibrium shape, and their growth leads to accumulation of the stresses associated with a crystallographic anisotropy and a difference in the density of the amorphous and crystalline phases. When increasing the size of the nanocrystals, the concentration of molybdenum in Ni (Mo) solid solution reduces, which, as previously noted, leads to increasing energy of stacking fault formation and, hence, decreasing the probability of twin formation by fluctuations of composition. On the other hand, molybdenum concentration in solid solution decreases during the growth of the nanocrystals; and its concentration increases at the reaction front (in the amorphous matrix in front of the crystal growing boundary). Details of the experimental observation of the distribution in front of the growing particle are given in [189].

In the processes of the primary crystallization the amorphous phase of Ni-based alloys is enriching in molybdenum. Naturally, the Mo concentration is increased near the growing nanocrystal and this increased concentration diminishes with the distance from the nanocrystal. Heterogeneities in the composition of the surrounded regions may be important for the origin of the twins or stacking faults near the nanocrystal boundary and its intergrowth into the nanocrystal. It should also be noted that by increasing the Mo concentration in the nickel lattice, stacking fault energy decreases, that is, formation of defects is facilitated. If these reasons, indeed, define the appearance of defects in the nanocrystals, you should expect the formation of twins and stacking faults in the near-boundary areas. The studies have shown that nanocrystals with defects in the near-boundary areas, in fact, present in the nanocrystalline structure. **Figure 16** shows a nanocrystal Ni(Mo) solid solution with defect-free central part and twins and stacking faults in the near-boundary regions.

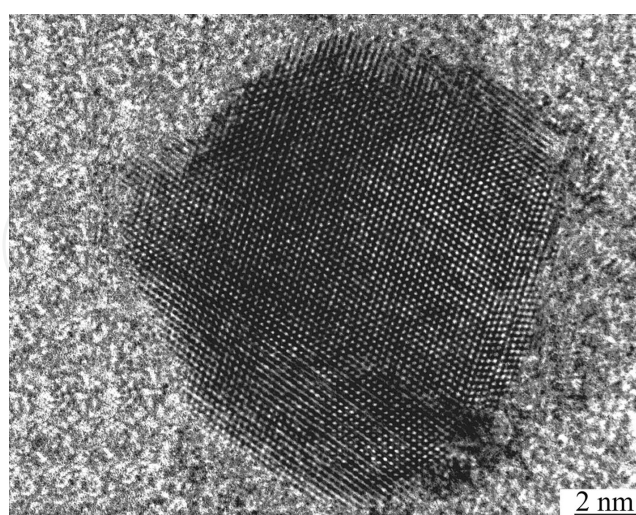


**Figure 16.** High-resolution electron microscopy image of the Ni(Mo) nanocrystal in the amorphous matrix.

Obviously, chemical heterogeneity is not only reason enough for the defects formation; small nanocrystals (up to  $\sim 5$  nm) are always defect-free. Formation of the crystals in the amorphous

matrix occurs in the field of stresses caused by the difference in specific volume per atom in the amorphous phase and in crystalline structure. Naturally, these stresses increase with the crystal sizes increasing. At the initial stages of crystal growth in isotropic amorphous phase these stresses are too small to induce the formation of defects in the nanocrystals. In the process of growth the nanocrystals reach the size when there is a growing stresses may cause the formation of defects.

It should be noted that the formation of microtwins and stacking faults cannot be determined by only size factor. One way of determining the degree of structure perfection of the nanocrystals formed in the amorphous phase was based on the following analysis of the diffraction line broadening:

- broadening of the diffraction line caused by the small grain size is proportional to  $1/\cos \theta$  or  $\sec \theta$  ( $\theta$  is the angle of the reflection);
- broadening of the diffraction line caused by randomly distributed dislocation is proportional to  $\tan \theta$ . If the nanocrystals do not contain defects, the half-widths of the diffraction reflections depend linearly on the secant of the diffraction angle. **Figure 17** shows such dependencies for Al-based alloy ( $\text{Al}_{82}\text{Ni}_{11}\text{Ce}_3\text{Si}_4$ ) and Ni-based alloy ( $(\text{Ni}_{70}\text{Mo}_{30})_{90}\text{B}_{10}$ ). These alloys contain the nanocrystals with practically the same size: 12 nm nanocrystals in  $\text{Al}_{82}\text{Ni}_{11}\text{Ce}_3\text{Si}_4$  and 13 nm in  $(\text{Ni}_{70}\text{Mo}_{30})_{90}\text{B}_{10}$ . Therefore, curves 1 (for  $\text{Al}_{82}\text{Ni}_{11}\text{Ce}_3\text{Si}_4$  alloy) and 2 (for  $(\text{Ni}_{70}\text{Mo}_{30})_{90}\text{B}_{10}$  alloy) correspond to two nanocrystalline alloys containing nanocrystals with approximately the same size ( $\sim 13$  nm). (It should be noted that the lattice parameter of the aluminum and nickel varies markedly, which determines the different quantities of points in the curves.) It is evident that a linear relationship is indeed characteristic of nanocrystals in an aluminum alloy, while linear dependence was not observed for nickel-based alloy. This means that the nanocrystals of the same size may be defect-free or contain linear defects in the different systems.

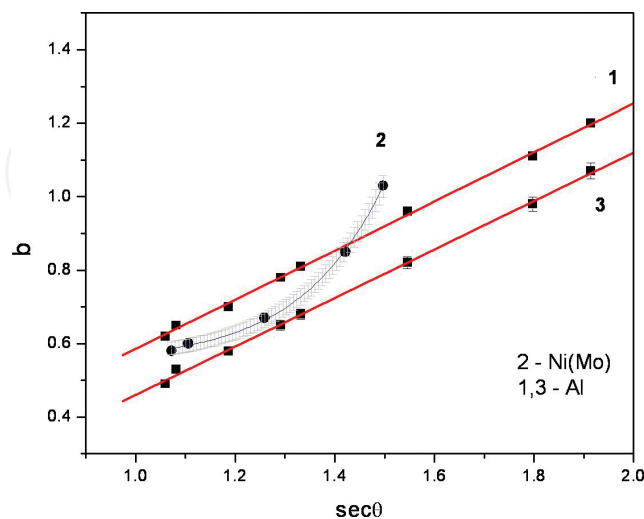


**Figure 17.** The angular dependence  $b$  of the diffraction line half-width (1 -  $\text{Al}_{82}\text{Ni}_{11}\text{Ce}_3\text{Si}_4$ , 2 -  $(\text{Ni}_{70}\text{Mo}_{30})_{90}\text{B}_{10}$ , 3 -  $\text{Al}_{88}\text{Ni}_{10}\text{Y}_2$ ).

However, it is more correct to compare the nanocrystals with the same size, expressed in the Burgers vector units (i.e., with the same number of interatomic distances); these values are  $42b$  and  $52b$  for curves 1 and 2, respectively. Therefore, for comparison, the figure also shows curve 3 corresponding to  $Al_{88}Ni_{10}Y_2$  alloy with the nanocrystal size of  $\sim 50b$ . As seen from the figure, in this case, the dependence (curve 3) is also linear, indicating that the broadening of the diffraction lines is caused by size factor only, that is, nanocrystals are defect-free. Thus, the size factor is not the only reason that determines the occurrence of defects in the nanocrystals; heterogeneities in composition play an important role as well.

In connection with the above, one point should be noted. As already mentioned, some researchers have suggested that there is a certain critical size of the nanocrystal, below which it is defect-free. For each such material critical size of the nanovolume can be estimated when a probability of the existence of induced defect sharply decreases [170]. Since the yield strength and elastic modulus for nickel are much larger (about three times) than that for aluminum, one would expect that the critical size of dislocation-free Al nanocrystals will be lower than that for Ni nanocrystals, but the experimental results do not match. The results show that the size of the nanocrystal, whereby there occur defects, actually, is different for different systems. It depends both on the chemical composition and concentration of the components and on the conditions of nanocrystal formation; one would expect that the formation of the nanocrystal, for example, in thin sections the size of defect-free crystal should be reduced significantly because the proximity surface will contribute to the resulting stress.

Obviously, to estimate perfection of the nanocrystalline structure, one should consider both the size of the crystals and the possible chemical heterogeneity, facilitating the formation of defects. The second factor is rather significant for nanocrystals comprising two or more components, the first one is important for any type of nanocrystals.

## 11. Structure design

As noted above, the changes occurring in the amorphous phase structure before the onset of crystallization may significantly affect the morphology and parameters of the crystalline structure forming on subsequent heating [116, 190, 191]. The amorphous phase is the parent phase for nanocrystals, which are formed by thermal and/or deformation effects. By varying the type and effect parameters, one can create amorphous-nanocrystalline materials with different size and volume fraction of nanocrystals. Nanocrystal formation usually occurs by the primary crystallization mechanism. This reaction leads to change of the amorphous phase composition and to enrich the amorphous phase in refractory components and metalloids. This process can result in an increased stability of the amorphous phase. The crystallization process thus can stop, and the resulting amorphous-nanocrystalline composites have high thermal stability. Heterogeneities in the amorphous phase may lead to the formation of different crystal phases. The noted structural changes do not exhaust all the possibilities for transformation of the system toward the equilibrium state. This wide variety of structures defines a set of good physical and chemical properties. For example, [116] annealing of amorphous Fe-B alloy at

temperatures below the crystallization temperature was found to alter microhardness and stability of the amorphous phase and ten-fold increase of the crystal size after subsequent crystallization. It has been found that heat treatment at different temperature ranges leads not only to a change of the phase composition but also to the formation of the structure with substantially smaller crystals upon subsequent heating. Formation of smaller crystals was also observed in the case of crystallization of heterogeneous amorphous structure. This last point is particularly important because it indicates the possibility of structure design, based on the decomposition and separation inside amorphous phase. The separation of amorphous phase makes it possible to produce amorphous samples with crystalline surfaces (**Figure 18**) and crystalline samples with amorphous surface (**Figure 19**) in Fe-B-P alloys [190].

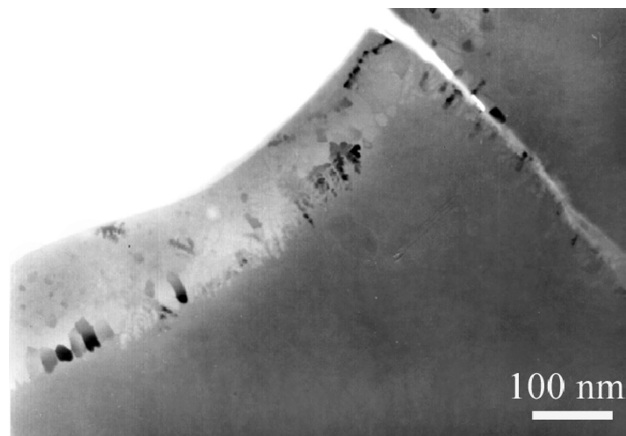


**Figure 18.** Microstructure of partially crystallized in-situ  $\text{Fe}_{83}\text{B}_{10}\text{P}_7$  alloy.



**Figure 19.** Microstructure of annealed and partially crystallized in-situ  $\text{Fe}_{83}\text{B}_{10}\text{P}_7$  alloy.

As most properties are structure-sensitive, the knowledge of the ways for structure design leads to the possibility of forming materials with the desired properties. Creating new materials with good properties, as already mentioned, is one of the major challenges of modern science.

## Author details

Galina Abrosimova\* and Alexandr Aronin

\*Address all correspondence to: gea@issp.ac.ru

Institute of Solid State Physics RAS, Chernogolovka, Russia

## References

- [1] Willens RH, Klement W, Duwez P. Continuous series of metastable solid solutions in silver-copper alloys. *J. Appl. Phys.* 1960; 31: 1136-1137.
- [2] Miroshnichenko IS, Sally IV. Device for crystallization of the alloys with high cooling rate. *Factory Lab.* 1959; 11: 1398-1399 (Rus.)
- [3] Skakov YuA, Kraposhin VS. Solidification at rapid cooling and phase transformation at heating of metallic glasses. *Metallovedenie i Termichaskaya Obrabotka.* 1980; 13: 3-78
- [4] He J, Zhou L, Zhao DL, Wang XL. Hysteresis loop shift behavior of CoFeSiB amorphous ribbons. *J. Mater. Res.* 2009; 24: 1607-1610
- [5] Fukunaga T, Ichikawa T, Suzuki K. Amorphous Magnetism II. In: Levy RA, Hasegawa R, Editors. New York: Plenum Press, 1977. p. 52
- [6] Suzuki K, Fujimori H, Hashimoto K. Amorphous Metals. Moscow: Metallurgy; 1987. 328 p.
- [7] Cahn RW. *Physical Metallurgy*. 3rd ed. Amsterdam: North-Holland Physics Publishing. 1983. 2. 624 p.
- [8] Uhlman BR. A kinetic treatment of glass formation. *J. Non-Cryst. Sol.* 1972; 7: 337-342
- [9] Du XH, Huang JC, Liu CT, Lu ZP. New criterion of glass forming ability for bulk metallic glasses. *J. Appl. Phys.* 2007; 101: 086108
- [10] Nagel SR, Tauc J. Correlations in binary liquid and glassy metals. *Solid State Commun.* 1977; 22: 129
- [11] Drehman AJ, Greer AL, Turnbull D. Bulk formation of a metallic glasses: Pd<sub>40</sub>Ni<sub>40</sub>P<sub>20</sub>. *Appl. Phys. Lett.* 1982; 41: 716
- [12] Molokanov VV, Chebotnikov VN. Glass Forming Ability, Structure and Properties of Ti and Zr-Intermetallic Compound Based Alloys. *Key. Eng. Mater.* 1990; 40-41: 319
- [13] Zhang T, Inoue A, Masumoto T. Amorphous Zr-Al-TM (Co=TM, Ni, Materials) Alloys with Significant Supercooled Liquid Region. *Mater. Trans. JIM.* 1991; 32: 1005

- [14] Lad'yanov VI, Sterkhova IV, Kamaeva LV, Molokanov VV. On the solidification of the Fe<sub>50</sub>Cr<sub>15</sub>Mo<sub>14</sub>C<sub>15</sub>B<sub>6</sub> bulk-amorphized alloy. *J. Non-Cryst. Sol.* 2010; 356:65-71
- [15] Abrosimova GE, Aronin AS, Matveev DV. Formation and structure of nanocrystals in bulk Zr<sub>50</sub>Ti<sub>16</sub>Cu<sub>15</sub>Ni<sub>19</sub> metallic glass. *Phys. Sol. State.* 2004; 46:2191-2195
- [16] Molokanov V, Petrzhik MI, Mikhailova TN, et al. Formation of bulk(Zr, Ti)-based metallic glass. *J. Non-Cryst. Sol.* 1999; 250:560-565
- [17] Abrosimova GE, Aronin AS, Kabanov YP, et al. Magnetic structure and properties of a bulk Fe<sub>72</sub>Al<sub>5</sub>P<sub>10</sub>Ga<sub>2</sub>C<sub>6</sub>B<sub>4</sub>Si<sub>1</sub> alloy in the amorphous and nanocrystalline states. *Phys. Sol. State.* 2004; 46: 885-890
- [18] Molokanov VV, Petrzhik MI, Mikhailova TN et al. Supercooled liquid region in Zr-Cu based bulk amorphous alloys. *J. Non-Cryst. Sol.* 1996; 207: 508-513
- [19] Zhang Q-D, Wang L-F, Zhao Y. Remarkable improving plasticity of a brittle Zr-based bulk metallic glass by a high rheological rate forming method in centesimal seconds. *Mater. Lett.* 2016; 164: 348-352
- [20] Ning Z, Liang W, Zhang M. High tensile plasticity and strength of a CuZr-based bulk metallic glass composite. *Mater. Des.* 2016; 90: 145-150
- [21] Chen YH, Huang JC, Du XH, et al. Time-dependent creep behavior of amorphous ZrCu and nanocrystalline Zr thin films—a comparison. *Intermetallics* 2016; 68: 101-106
- [22] Abrosimova GE, Aronin AS, Kabanov YP, et al. Magnetic structure and properties of a bulk Fe<sub>72</sub>Al<sub>5</sub>P<sub>10</sub>Ga<sub>2</sub>C<sub>6</sub>B<sub>4</sub>Si<sub>1</sub> alloy in the amorphous and nanocrystalline states. *Phys. Sol. State.* 2004; 46: 885-890
- [23] Abrosimova GE, Aronin AS, Matveev DV, Molokanov VV. Formation and structure of nanocrystals in bulk Zr<sub>50</sub>Ti<sub>16</sub>Cu<sub>15</sub>Ni<sub>19</sub> metallic glass. *Phys. Sol. State.* 2004; 46: 2191-2195
- [24] Halation S, Haddad-Sabzevar M. Thermal stability and non-isothermal crystallization kinetics of Ti<sub>41.5</sub>Cu<sub>42.5</sub>Ni<sub>7.5</sub>Zr<sub>2.5</sub>Hf<sub>5</sub>Si<sub>1</sub> bulk metallic glass. *J. Non-Cryst. Sol.* 2015; 429: 164-170
- [25] Skryshevskii AF, *Structure Analysis of Liquids and Amorphous Solids.* Moscow: High School; 1980
- [26] Romanova AV, Illinskii AG. *Amorphous Metallica Alloys.* Kiev: Naukova Dumka; 1987. 248 p. (Rus.)
- [27] *Glassy Metals II. Atomic Structure and Dynamics, Electronic Structure, Magnetic Properties.* Ed. H. Beck, H.-J. Güntherodt. Berlin: Springer-Verlag; 1983. 454 p.
- [28] Abrosimova GE, Matz W. Construction of partial structural functions of amorphous Fe<sub>84</sub>B<sub>16</sub> alloys by means of neutron diffraction. *Phys. Met.* 1989; 11:36-43 (in Russian)

- [29] Waseda Y. *The Structure of Liquids, Amorphous Solids and Solid Fast Ion Conductors*. Pergamon Press. 1981. 122 p.
- [30] Matz W, Hermann H, Mattern N. On the structure of amorphous Fe<sub>75</sub>B<sub>25</sub>. *J. Non-Cryst. Sol.* 1987; 93: 217-229
- [31] Bhatia AB, Thornton DE. Structural aspects of the electrical resistivity of binary alloys. *Phys. Rev. B.* 1970; 2: 3004-3012
- [32] Mattern N, Kühn U, Hermann H, Ehrenberg H, Neufeind J, Eckert J. Short range order of Zr<sub>62-x</sub>Ti<sub>x</sub>Al<sub>10</sub>Cu<sub>20</sub>Ni<sub>8</sub> bulk metallic glasses. *Acta Mater.* 2002; 50: 305-314
- [33] Cheng YQ, Ma E. Atomic-level structure and structure–property relationship in metallic glasses. *Prog. Mater. Sci.* 2011; 56:379–473
- [34] Svergun DI, Feigin LA. *X-ray and Neutron Small Angle Scattering*. Moscow: Nauka; 1986. 280 p. (Rus.)
- [35] Sheng HW, Luo WK, Alamgir FM, Bai JM, Ma E. Atomic packing and short-to-medium range order in metallic glasses. *Nature.* 2006; 439:419-425
- [36] Li Huang, Wang CZ, Hao SG, Kramer MJ, Ho KM. Atomic size and chemical effects on the local order of Zr<sub>2</sub>M (M=Co, Ni, Cu, and Ag) binary liquids. *Phys. Rev. B.* 2010; 81: 014108
- [37] Hirata A, Guan P, Fujita T, Hirotsu Y, Inoue A, Yavari AR, Sakurai T, Chen M. Direct observation of local atomic order in a metallic glass. *Nat. Mater.* 2011; 10:28-33
- [38] Liebermann HH, Graham CD, Jr., Flanders PJ. Changes in Curie temperature, physical dimensions, and magnetic anisotropy during annealing of amorphous magnetic alloys. *IEEE. Trans. Magn.* 1977; 13:1541
- [39] Abrosimova GE, Serebryakov AV, Sokolovskaya ZhD. Change of structure and properties of Fe-based metal-metalloid amorphous alloys at heat treatment. *Fizika Metallov I Metallovedenie.* 1988; 66:727
- [40] Ray R, Giessen BC, Grant NJ. New non-crystalline phases in splat cooled transition metal alloys. *Scr. Met.* 1968; 2:359
- [41] Pokatilov VS. NMR-study of atomic-structure in amorphous FeB-alloys. *Dokl. Akad. Nauk. SSSR* 275 (1984) 79-83
- [42] Ichikawa T. The assembly of hard spheres as a structure model of amorphous iron. *Phys. Stat. Sol.* 1975; a29:293-302
- [43] Polk DE. Structural model for amorphous metallic alloys. *Scr. Met.* 1970; 4:117
- [44] Yamamoto R, Matsuoka H. Relaxed bernal structure as a model of amorphous iron. *J. Phys. F: Met. Phys.* 1978; 7: L243

- [45] Bernal JD. The Bakerian Lecture. 1962. The Structure of Liquids. London: Proc. Roy. Soc. (London). 1964; 280A:299-322
- [46] Wang R. Short-range structure for amorphous intertransition metal alloys. *Nature*. 1979; 278: 700
- [47] Egami T et al. Structure of bulk amorphous Pd–Ni–P alloys determined by synchrotron radiation. *Metall. Mater. Trans. A, Phys. Met. Mater. Sci.* 1998; 29(7):1805–1809
- [48] Miracle DB. The efficient cluster packing model—an atomic structural model for metallic glasses. *Acta Mater.* 2006; 54(16): 4317–4336
- [49] Sheng HW, Cheng YQ, Lee PL, Shastri SD, Ma E. Atomic packing in multicomponent aluminum-based metallic glasses. *Acta Mater.* 2008; 56(20): 6264–6272
- [50] Sheng HW et al. Atomic packing and short-to-medium-range order in metallic glasses. *Nature*. 2006; 439(7075): 419–425
- [51] Lu BC et al. A model of atom dense packing for metallic glasses with high-solute concentration. *Appl. Phys. Lett.* 2009; 94(24):241913
- [52] Ma D, Stoica AD, Wang XL. Power-law scaling and fractal nature of medium-range order in metallic glasses. *Nat. Mater.* 2009; 8(1):30–34
- [53] Abrosimova GE, Aronin AS. Evolution of the amorphous-phase structure in metal-metal type metallic glasses. *J. Surf. Investig. X-ray Synchtr Tech* 2015; 9(5):887–893
- [54] Chou C-P, Turnbull D. Transformation behavior of Pd-Au-Si metallic glasses. *J. Non-Cryst. Sol.* 1975; 17:169
- [55] Chen HS. Mater Glass temperature, formation and stability of Fe, Co, Ni, Pd and Pt based glasses. *Sci. Eng.* 1976; 23:151-154
- [56] Tanner L, Ray R. Physical properties of Ti<sub>50</sub>Be<sub>40</sub>Zr<sub>10</sub> glass. *Scr. Met.* 1980; 11:783-789
- [57] Inoue A, Yamamoto M, Kimura HM, Masumoto T. Ductile aluminum-base amorphous alloys with two separate phases. *J. Mater. Sci.* 1987; 6:194
- [58] Yavari AR. On the structure of metallic glasses with double diffraction halos. *Acta Met.* 1988; 36:1863
- [59] Marcus M. Phase separation and crystallization in amorphous Pd-Si-Sb. *J. Non-Cryst. Sol.* 1979; 30:317
- [60] Cohen MH, Turnbull D. Molecular transport in liquids and glasses. *J. Chem. Phys.* 1959; 31:1164-1169
- [61] Chen HS, Turnbull D. Formation, stability and structure of palladium-silicon based alloy glasses. *Acta Met.* 1969; 17:1021
- [62] Mehra M, Schulz R, Johnson WL. Structural studies and relaxation behavior of (Mo<sub>0.6</sub>Ru<sub>0.4</sub>)<sub>100-x</sub>B<sub>x</sub> metallic glasses. *J. Non-Cryst. Sol.* 1984; 61-62:859

- [63] Nagarajan T, Asari UCh, Srinivasan S, Sridharan V, Narayanasamy A. Amorphous phase separation in METGLAS 2605CO. *Hyperfine Interact.* 1987; 34:491
- [64] Mak A, Samwer K, Johnson WL. Evidence for two distinct amorphous phases in  $(\text{Zr}_{0.667}\text{Ni}_{0.333})_{1-x}\text{B}_x$  alloys. *Phys. Lett.* 1983; 98A:353
- [65] Doi K, Kayano H, Masumoto T. Small-angle scattering from neutron-irradiated amorphous  $\text{Pd}_{80}\text{Si}_{20}$ . *J. Appl. Cryst.* 1978; 11:605
- [66] Terauchi H. Heterogeneous structure of amorphous materials. *J. Phys. Soc. Jpn.* 1983; 52:3454 -3459
- [67] Osamura K. Structure and mechanical properties of a  $\text{Fe}_{90}\text{Zr}_{10}$  amorphous alloy. *J. Mater. Sci.* 1984;19:1917
- [68] Hermann H, Mattern N, Kuhn U, Heinemann A, Lazarev NP. Evolution of spatial heterogeneity in a Zr-based metallic glass. *J. Non-Cryst. Sol.* 2003; 317: 91-96
- [69] Osamura K. SAXS study on the structure and crystallization of amorphous metallic alloys. *Colloid. Polym Sci.* 1981; 259:677
- [70] Sheng HW et al. Polyamorphism in a metallic glass. *Nat. Mater.* 2007; 6(3):192–197
- [71] Egami T, Vitek V, Srolovitz D. Microscopic model of structural relaxation in amorphous alloys. *Proc. 4th Int. Conf. on Rapidly Quenched Metals (Sendai 1981)* /ed. Masumoto T, Suzuki K. Sendai: Institute of Metals. 1982. p. 2
- [72] Scott MG, Kursumovic A. Short-range ordering during structural relaxation of the metallic glass  $\text{Fe}_{40}\text{Ni}_{40}\text{B}_{20}$ . *Acta Met.* 1982; 30:853
- [73] Shiga M. Magnetovolume: effects in ferromagnetic transition metals. *J. Phys. Soc. Jpn.* 1981; 50:2573 -2580
- [74] Egami T. Structural relaxation in amorphous alloys— compositional short range ordering. *Mater. Res. Bull.* 1978; 13:557
- [75] Masumoto T, Maddin R. Structural stability and mechanical properties of amorphous metals. *Mater. Sci. Eng.* 1975; 19:1 -24
- [76] Chen HS. Glassy metals. *Rep. Prog. Phys.* 1980; 43:353
- [77] *Ultrarapid Quenching of Liquid Alloys.* Ed, H. Hermann. New York: Academic Press; 1981. 375 p.
- [78] Richardson MJ, Savill NG. Derivation of accurate glass transition temperatures by differential scanning calorimetry. *Polymer.* 1975;16:753-757
- [79] Harmelin M, Calvayrac Y, Quivy A, Chevalier JP, Bigot J. On the effect of the initial quench on the thermal behaviour of amorphous  $\text{Cu}_{60}\text{Zr}_{40}$  alloys. *Scr. Met.* 1982;16:707
- [80] Greer AL. Crystallization kinetics of  $\text{Fe}_{80}\text{B}_{20}$  glass. *Acta Met.* 1982; 30:171

- [81] Chambron W, Chamberod A. Reversible enhancement of magnetic directional ordering rate associated with quenched-in defects, in an amorphous  $\text{Fe}_{40}\text{Ni}_{38}\text{Mo}_4\text{B}_{18}$  alloy. *Solid State Commun.* 1980; 35:61
- [82] Argon AS. Plastic-deformation in metallic glasses. *Acta Met.* 1979; 27:47–58
- [83] Pampillo CA, Chen HS. Comprehensive plastic deformation of a bulk metallic glass. *Mater. Sci. Eng.* 1974; 13:181
- [84] Neihauser G, Stossel RP. Homogeneous and Heterogeneous Deformation of metallic glasses. In: *Rapid Quenching metallic alloys*. Ed. Steeb S, Warkimont G. Moscow: Metallurgy; 1989 p. 247-252 (Rus.)
- [85] Spaepen F. A microscopic mechanism for steady state inhomogeneous flow in metallic glasses. *Acta Met.* 1977; 25:407
- [86] Chen H., Huang JG, Song SX, Nieh TG, Jang JSC. Flow serration and shear-band propagation in bulk metallic glasses. *Appl. Phys. Lett.* 2009; 94:141914
- [87] Georgarakis K. Shear band melting and serrated flow in metallic glasses. *App. Phys. Lett.* 2008; 93:031907
- [88] Handrich K, Kobe S. *Amorphous Ferro- and Ferrimagnetics*. Moscow: Mir; 1982. 106 c. (Rus.)
- [89] Masumoto T. Mechanical characteristics of amorphous metals. *Sci Repts. RITU.* 1977; A26: 246-262.
- [90] Zolotukhin IV, Khonik VA, Safonov IF. Strength, plasticity and stress relaxation in amorphous  $\text{La}_{80}\text{Al}_{20}$  alloy. *Fizika i chimiya stekla.* 1983; 9: 67-73 (Rus).
- [91] Ashby MF, Greer AL. Metallic glasses as structural materials. *Scr. Mater.* 2006; 54: 321-326.
- [92] Ichitsubo T. Nanoscale elastic inhomogeneity of a Pd-based metallic glass: sound velocity from ultrasonic and inelastic X-ray scattering experiments. *Phys. Rev. B.* 2007; 76: 140201.
- [93] Srolovitz D, Vitek V, Egami T. An atomistic study of deformation of amorphous metals. *Acta Met.* 1983; 31: 335–352
- [94] Bulatov V.V., Argon A.S. A stochastic-model for continuum elastoplastic behavior. 1. Numerical approach and strain localization. *Model Simul. Mater. Sci. Eng.* 1994; 2: 167–184.
- [95] Johnson WL, Samwer K. A universal criterion for plastic yielding of metallic glasses with a  $(T/T_g)^{2/3}$  temperature dependence. *Phys. Rev. Lett.* 2005; 95: 195501.
- [96] Cheng YQ, Sheng HW, Ma E. Relationship between structure, dynamics, and mechanical properties in metallic glassforming alloys. *Phys. Rev. B.* 2008; 78: 014207.

- [97] Krebs HU, Biegel W, Bienenstock A. Phase separation in amorphous Zr-Fe alloys determined by anomalous X-ray scattering and magnetization measurements. *Mater. Sci. Eng.* 1988; 97: 163-7
- [98] G. Abrosimova, A. Aronin, A. Budchenko. Amorphous phase decomposition in Al-Ni-RE system alloys. *Mater. Lett.* 2015; 139: 194-196
- [99] Abrosimova GE, Aronin AS. Effect of the concentration of a rare earth component on the parameters of the nanocrystalline structure in aluminum-based alloys. *Phys. Sol. State.* 2009; 51: 1765-1771
- [100] Abrosimova GE, Aronin AS, Ignat'eva EYu, Molokanov VV. Phase decomposition and nanocrystallization in amorphous  $\text{Ni}_{70}\text{Mo}_{10}\text{P}_{20}$  alloy. *JMMM.* 1999; 203: 169-171
- [101] Abrosimova G, Aronin A, Ignatieva E. Decomposition of amorphous phase in  $\text{Ni}_{70}\text{Mo}_{10}\text{B}_{20}$  alloy above glass transition temperature. *Mater. Sci. Eng.* 2007; A449-451: 485-488
- [102] Abrosimova GE, Aronin AS. Specific features of amorphous  $\text{Fe}_{90}\text{Zr}_{10}$  alloy separation upon heating. *Phys. Sol. State.* 1998; 40: 1603-1606.
- [103] Naudon A, Flank V. Relationship between space correlated fluctuations and initial alloy composition in some metallic glasses. *J. Non-Cryst. Sol.* 1984; 61/62: 355-360
- [104] Abrosimova GE, Aronin AS, Asadchkov VE, Serebryakov AV. Structure evolution of Fe-B and Co-Fe-Si-B alloys during heating below crystallization temperature. *Fizika metallov i metallovedenie.* 1986; 62: 496-502
- [105] Abrosimova GE, Aronin AS. Reversible structural changes on heat treatment of amorphous Fe-B alloys. *Int. J. Rapid Sol.* 1991; 6: 29-40
- [106] Elliot PR. *Constitution of Binary Alloys. First Supplement.* NY: McGraw-Hill Book Company; 1970. 472 p.
- [107] Pampillo CA. Flow and fracture in amorphous alloys. *J. Mater. Sci.* 1975; 10: 1194-1197.
- [108] Zeng QS. Anomalous compression behavior in lanthanum/cerium-based metallic glass under high pressure. *Proc. Natl. Acad. Sci. USA.* 2007; 104(34): 13565-13568.
- [109] Wang XD, Bednarcik J, Saksi K, Franz H, Cao QP, Jiang JZ. Tensile behavior of bulk metallic glasses by *in situ* X-ray diffraction. *Appl. Phys. Lett.* 2007; 91: 081913.
- [110] Stoica M, Das J, Bednarcik J, Franz H, Mattern N, Wang WH, Eckert J. Strain distribution in  $\text{Zr}_{64.13}\text{Cu}_{15.75}\text{Ni}_{10.12}\text{Al}_{10}$  bulk metallic glass investigated by *in situ* tensile tests under synchrotron radiation. *J. Appl. Phys.* 2008; 104: 013522.
- [111] Wang XD, Bednarcik J, Franz H, Lou HB, He ZH, Cao QP, Jiang JA. Local strain behavior of bulk metallic glasses under tension studied by *in situ* X-ray diffraction. *Appl. Phys. Lett.* 2009; 94: 011911

- [112] Abrosimova GE, Aronin AS, Afonikova NS, Kobelev NP. Effect of the deformation on structure change of amorphous Pd<sub>40</sub>Ni<sub>40</sub>P<sub>20</sub> phase. *Phys. Sol. State.* 2010; 52: 1892
- [113] Suzuki K. Small Angle and Very-Small Angle X-Ray Scattering from Amorphous Pd<sub>80</sub>Si<sub>20</sub> before and after Cold Work. *Jpn. J. Appl. Phys.* 1981; 20: 271
- [114] Walter J. J. Crystallization of the amorphous alloys Fe<sub>50</sub>Ni<sub>30</sub>B<sub>20</sub> and Fe<sub>80</sub>oB<sub>20</sub>. *Mater. Sci. Eng.* 1977; 29: 161
- [115] Shirnina DP, G.E. Abrosimova, A.S. Aronin nanocrystal formation in Al-based alloys at the deformation. *Des. Mater. Technol.* 2011; 3(18): 80 (Rus.).
- [116] Abrosimova GE, Aronin AS, Bezrukov AV, Pankratov SP, Serebryakov AV. Effect of heat treatment conditions on crystallization of amorphous Fe-B alloys. *Phys. Met.* 1982; 4: 114
- [117] Zhukov AP, Ponomarev BK. Dependence of the start field on the frequency and amplitude of remagnetizing field in Fe and Co based amorphous alloys. *Fizika Tverdogo Tela.* 1989; 31: 26-30
- [118] Abrosimova GE, Zhukov AP, Ponomarev BK. Effect of heat treatment on some properties of Fe- and Co-based amorphous alloys. *Phys. Stat. Sol.* 1989; 111a: K237-K241
- [119] Walter JL, Bacon F, Luborsky FE. *Mater. Sci. Eng.* 1976; 24: 239
- [120] Herold U., Koster U. in *Proceedings of the Third International Conference on Rapidly Quenched Metals.* ed. by Cantor B., Brighton, Metals Society. London; 1978. V. 1. 281 p.
- [121] Freed RL, VaderSande JB. The metallic glass Cu<sub>56</sub>Zr<sub>44</sub>: devitrification and the effects of devitrification on mechanical properties. *Acta Met.* 1980; 28: P. 103
- [122] Rawson H. *Inorganic Glass-Forming Systems.* London: Academic Press. 1967.
- [123] Fine ME. *Phase Transformation in Condensed Systems.* New York: MacMillan. 1964.
- [124] Birac C, Lesueur D. Diffusion atomique du lithium dans l'alliage métallique amorphe Pd-Si. *Phys. Status Solidi.* 1976 ; 36a: 247.
- [125] Köster U, Herold U. *Metallic Glasses in Glassy Metals.* Ed. H. Beck, H.-J. Güntherodt. Berlin: Springer-Verlag. 1983. 454 p.
- [126] Martin JW, Doherty RD. *Stability of Microstructure in Metallic Systems.* Cambridge: Cambridge University Press. 1976. 280 p.
- [127] Ham RK, Kirkaldy JS, Plewes JW. The fatigue of Cu-Ni-Fe alloys. *Acta Met.* 1967; 15: 861-869.
- [128] Chen HS, Turnbull D. Formation, stability and structure of palladium-silicon based alloy glasses. *Acta Met.* 1969; 17: 1021

- [129] Stoering R, Conrad H, Metastable structures in liquid quenched and vapor quenched Ag-Cu alloys. *Acta Met.* 1969; 17: 933
- [130] Mattern N, Goerigk G, Vainio U, Miller MK, Gemming T, Eckert J. Spinodal decomposition of Ni-Nb-Y metallic glasses. *Acta Mater.* 2009; 57: 903-908.
- [131] Aronin AS, Serebryakov AV. Volume Discrepancy Compensation Upon Crystallization of Some Amorphous Alloys. Chernogolovka: ISSP. 1981. 9 p. (Rus).
- [132] Yoshizawa Y, Oguma S, Yamauchi K. New Fe-based soft magnetic alloys composed of ultrafine grain structure. *J. Appl. Phys.* 1988; 64: 6044.
- [133] Khan Y, Sostarich M. Dynamic temperature X-ray diffraction analysis of amorphous  $\text{Fe}_{80}\text{B}_{20}$ . *Z. Met.* 1981; 72: 266-268.
- [134] Herold U., Koster U. Metastabile Phasen in extreme schnell erstarrten Eisen-Bor-Legierungen. *Z. Met.* 1978; 69: 326-332.
- [135] Abrosimova GE, Serebryakov AV. Metastable phase decomposition in Fe-B alloys. *Phys. Met.* 1983; 5: 85-88
- [136] Inal OT, Kekker L, Yost FG. High-temperature crystallization behavior of amorphous  $\text{Fe}_{80}\text{B}_{20}$ . *J. Mater. Sci.* 1980; 15: 1947-1961
- [137] Khan Y. Sostarich M. Dynamic temperature X-ray diffraction analysis of amorphous  $\text{Fe}_{80}\text{B}_{20}$ . *Z. Metallk.* 1981; 72: 266-268
- [138] Abrosimova GE, Aronin AS, Gantmakher VF, Levin YuB, Osherov MV. Variation of the electrical resistivity of the amorphous Ni-Zr alloy in the initial-stages of crystallization. *Fizika Tverdogo Tela.* 1988; 30: 1424-1430.
- [139] Abrosimova GE, Aronin AS, Zverkova II, Kir'yanov YuV, Molokanov VV. Early stages of amorphous  $\text{Zr}_{65}\text{Cu}_{17.5}\text{Ni}_{10}\text{Al}_{7.5}$  alloy crystallization. *Fizika metallov I metallovedenie.* 1998; 86: 91-96
- [140] Abrosimova GE, Aronin AS, Matveev DV, Molokanov VV. Formation and structure of nanocrystals in bulk  $\text{Zr}_{50}\text{Ti}_{16}\text{Cu}_{15}\text{Ni}_{19}$  metallic glass. *Fizika Tverdogo Tela.* 2004; 46: 2191-2195
- [141] Abrosimova GE, Aronin AS, Kir'janov YuV, Matveev DV, Zver'kova II, Molokanov VV, Pan S, Slipenyuk A. The structure and mechanical properties of bulk  $\text{Zr}_{50}\text{Ti}_{16.5}\text{Cu}_{14}\text{Ni}_{18.5}$  metallic glass. *J. Mater. Sci.* 2001; 36: 3933-3939,
- [142] Abrosimova GE, Kobelev NP, Kolyvanov EV, Khonik VA. The influence of heat treatment on the ultrasonic velocity and elastic moduli of a Zr-Cu-Ni-Al-Ti bulk metallic glass. *Phys. Sol. State.* 2004; 46: 1859-1862
- [143] Abrosimova GE, Kobelev NP, Kolyvanov EV, Khonik VA, Levin VM. Effect of heat treatment on elastic characteristics of a bulk amorphous Zr-Cu-Ni-Al-Ti alloy. *Phys. Sol. State.* 2006; 48: 2091-2094

- [144] Frankwicz PS, Ram S, Fecht H-J. Enhanced microhardness in Zr<sub>65.0</sub>Al<sub>17.5</sub>Ni<sub>10.0</sub>Cu<sub>17.5</sub> amorphous rods on coprecipitation of nanocrystallites through supersaturated intermediate solid phase particles. *Appl. Phys. Lett.* 1996; 68: 2825
- [145] Köster U, Meinhardt J, Roos S, Liebertz H. Formation of quasicrystals in bulk glass forming Zr–Cu–Ni–Al alloys. *Appl. Phys. Lett.* 1996; 69: 179
- [146] Xing LQ, Eckert J, Löser W, Schultz L. High-strength materials produced by precipitation of icosahedral quasicrystals in bulk Zr–Ti–Cu–Ni–Al amorphous alloys. *Appl. Phys. Lett.* 1999; 74: 664.
- [147] Li CF Precipitation of icosahedral quasicrystalline phase in metallic glasses. *Appl. Phys. Lett.* 2000; 77: 528-530
- [148] Abrosimova GE, Aronin AS, Serebraykov AV. Structure of rapidly quenched Al-Mn alloys. *Suppl. Trans. JIM.* 1988; 29: 485-488.
- [149] He G, Löser W, Eckert J. Microstructure and mechanical properties of the Zr<sub>66.4</sub>Cu<sub>10.5</sub>Ni<sub>8.7</sub>Al<sub>8</sub>Ti<sub>6.4</sub>. *Scr. Mater.* 2003; 48: 1531-1536
- [150] Abrosimova GE, Aronin AS, Gurov AF. Formation and structure of light-weight nanocrystalline alloys of the aluminum-nickel-RE system. *Phys. Met. Metallogr.* 2000; 90: 180-185
- [151] Abrosimova GE, Aronin AS, Zverkova II. Phase transformation upon crystallization of amorphous Al-Ni-RE alloys. *Phys. Met. Metallogr.* 2002; 94: 102-107
- [152] Cremanshi V, Arcondo B, Sirkin H, Vazquez M, Asenjo F, Garcia JM, Abrosimova G, Aronin A. Huge magnetic hardening ascribed to metastable crystallites during first stages of devitrification of amorphous FeSiBNbSn alloys. *J. Mater. Res.* 2000; 15: 1936-1942,
- [153] Wang WK, Iwasaki H, Suryanaryana C, Masumoto T. Crystallization characteristics of an amorphous Ti<sub>80</sub>Si<sub>20</sub> alloy at high pressure. *J. Mater. Sci.* 1983; 18: 3765-3772.
- [154] Ogawa Y, Nunogaki K, Endo S, Kiritani M, Fujita FF. Crystallization of amorphous Fe-B alloys under pressure. *Sendai: Proc. 4th Int. Conf. on Rapidly Quenched Metals.* 1981. P. 675-678.
- [155] Steinhardt PJ. Solid-state physics – how does your quasicrystal grow? *Nature.* 2008; 452: 43
- [156] Kelton KF. First X-ray scattering studies on electrostatically levitated metallic liquids: demonstrated influence of local icosahedral order on the nucleation barrier. *Phys. Rev. Lett.* 2003; 90: 195504.
- [157] Shen YT. Icosahedral order, frustration, and the glass transition: evidence from time-dependent nucleation and supercooled liquid structure studies. *Phys. Rev. Lett.* 2009; 102: 057801.

- [158] Saida J. Precipitation of icosahedral phase from a supercooled liquid region in  $Zr_{65}Cu_{7.5}Al_{7.5}Ni_{10}Ag_{10}$  metallic glass. *Appl. Phys. Lett.* 1999; 75: 3497.
- [159] Gleiter H. Nanocrystalline materials. *Prog. Mater. Sci.* 1989; 33: 223-315
- [160] Birringer R. Nanocrystalline materials. *Mater. Sci. Eng.* 1989; A117: 33-43
- [161] Turnbull D, Cohen MH. On free-volume model of liquid-glass transition. *J. Chem. Phys.* 1970; 52: 30308
- [162] Zolotukhin IV. Physical properties of amorphous metallic materials. Moscow: Metallurgy. 1986. 176 p. (Rus)
- [163] Ramachandrarao P, Cantor B, Cahn RW. Viscous behavior of undercooled metallic melts. *J. Non-Cryst. Sol.* 1977; 24: 109
- [164] Ramachandrarao P, Cantor B, Cahn RW. Free volume theories of the glass transition and the special case of metallic glasses. *J. Mater. Sci.* 1977; 12: 2488
- [165] Cahn RW. Rapid Solidification Processing: Principles and Technologies, eds. R. Mehrabian et al. Clattor's. LA: Baton Rouge. 1978. 129 p.
- [166] Louzguine-Luzgin D, Inoue A. Nano-devitrification of glassy alloys. *J. Nanosci. Nanotechnol.* 2005; 5: 999-1014.
- [167] Yavari AR, Osamura K, Okuda H, Amemia Y. Small-angle x-ray scattering study of phase separation in amorphous alloys during heating with use of synchrotron radiation. *Phys. Rev. B.* 1988; 37: 7759-7765.
- [168] Inoue A, Yamamoto M, Kimura HM, Masumoto T. Ductile aluminium-base amorphous alloys with two separate phases. *J. Mater. Sci. Lett.* 1987; 6: 194.
- [169] Aronin AS, Abrosimova GE, Gurov AF, Kir'janov YuV, Molokanov VV. Nanocrystallization of bulk Zr-Cu-Ti metallic glass. *Mater. Sci. Eng.* 2001; A304-306: 375-379.
- [170] Gutkin MYu, Ovid'ko IA. Physical Mechanics of Deformed Nanostructures. S-Petersburg: Yanus, 2003. 194 p. (Rus).
- [171] Gryaznov VG, Trusov LI. Size effect in micromechanics of nanocrystals. *Prog. Mater. Sci.* 1993; 37: 290-400.
- [172] Gryaznov VG, Karepov AM, Romanov AE. Critical instability of dislocations in microcrystals. *Pisma v zhurnal tekhnicheskoi fiziki.* 1989. 15:39-44
- [173] Wang N, Wang Z, Aust KT, Erb U. Effect of grain size in the mechanical properties of nanocrystalline materials. *Acta Metall. Mater.* 1995; 43: 519.
- [174] Abrosimova GE, Aronin AS. Fine structure of FCC nanocrystals in Al- and Ni-based alloys. *Phys. Sol. State.* 2002; 44: 1003-1007
- [175] Abrosimova GE, Aronin AS. Size effect on the structure of Al- and Ni-based nanocrystals. *Phys. Sol. State.* 2008; 50: 159-163

- [176] Abrosimova GE, Aronin AS, Kir'janov YuV, Zver'kova II, Molokanov VV, Alves H, Köster U. The formation, structure and properties of nanocrystalline Ni-Mo-B alloys. *J. Mater. Sci.* 1999; 34: 1611-1618.
- [177] Aronin AS, Abrosimova GE, Zver'kova II, Kir'janov YuV, Molokanov VV, Petrzhik MI. The structure of nanocrystalline Ni<sub>58.5</sub>Mo<sub>31.5</sub>B<sub>10</sub> and structure evolution at heat treatment. *Mater. Sci. Eng.* 1997; A226-228: 536-540.
- [178] Abrosimova GE, Aronin AS, Zver'kova II, Gurov AF, Kir'janov YuV, Formation, structure and microhardness of nanocrystalline Ni-No-B alloys. *Phys. Sol. State.* 1998; 40: 8-13.
- [179] Aronin AS, Abrosimova GE, Kir'janov YuV. Formation and structure of nanocrystals in an Al<sub>86</sub>Ni<sub>11</sub>Yb<sub>3</sub> alloy. *Phys. Sol. State.* 2001; 43: 2003–2011
- [180] Abrosimova GE, Aronin AS, Barkalov OI, Dement'eva MM. Formation of the nanostructure in amorphous alloys of Al-Ni-Y system. *Phys. Sol. State.* 2013; 55: 1773-1778
- [181] Köster U., Schunemann M., in: *Rapidly Solidified Alloys*, ed. H.H. Liebermann, New York: Marcel Dekker Inc. 1993, 303p.
- [182] Ham FS, Theory of diffusion-limited precipitations. *J. Phys. Chem. Sol.* 1958; 6: 335 - 351
- [183] Hebert RJ, Boucharat N, Perepezko JM, Rösher H, Wilde G. *J. Alloys Compd.* 2007; 434-435: 18
- [184] Hirth JP, Lothe J, *Theory of Dislocations*. New York: McGraw-Hill Book Company. 1972
- [185] Gallagher PCJ. Thermodynamic of metal interstitial solution. *Trans. AIME.* 1970; 1: 2429
- [186] Howie A, Swann PR. Direct measurements of stacking-fault energies from observations of dislocation modes. *Phil Mag.* 1961; 6: 1215.
- [187] Kelly A, Groves GW, *Crystallography and Crystal Defects*. London: Longman. 1970. 470 p.
- [188] Bolling GF, Richman RH. Continual mechanical twinning: Part I: Formal description. *Acta Met.* 1965; 13: 709
- [189] Hono K. Atom probe microanalysis and nanoscale microstructures in metallic materials. *Acta Mater.* 1999; 47: 3127-3145
- [190] Aronin AS, Ivanov SA, Yakshin AE. Increase of the near-surface crystallization temperature in a Fe-B-P amorphous alloy. *Fizika Tverdogo Tela.* 1991; 33: 2527-2532
- [191] Abrosimova GE, Aronin AS. Effect of the concentration of a rare-earth component on the parameters of the nanocrystalline structure in aluminum-based alloys. *Phys. Sol. State.* 2009; 51: 1765-1771

